

Lappeenranta–Lahden teknillinen yliopisto LUT
LUT School of Energy Systems
LUT Mechanical Engineering

Juuso Narsakka

COUPLING DESIGN AND ANALYSIS FOR HIGH-SPEED DRIVETRAIN
SUPPORTED BY THREE ACTIVE MAGNETIC BEARINGS

14.4.2022

Examiner(s): Professor Jussi Sopanen
Professor Emil Kurvinen

TIIVISTELMÄ

Lappeenrannan–Lahden teknillinen yliopisto LUT
LUT School of Energy Systems
LUT Kone

Juuso Narsakka

Coupling Design and Analysis for High-Speed Drivetrain Supported by Three Active Magnetic Bearings

Diplomityö

2022

79 sivua, 37 kuvaa, 16 taulukko ja 1 liitettä

Tarkastajat: Professori Jussi Sopenen, LUT-yliopisto
Professori Emil Kurvinen, Oulun yliopisto

Hakusanat: Suurnopeus sähkömoottori, kytkimen suunnittelu, roottoridynamiikka

Suurnopeuskoneet ovat operoineet korkealla hyötysuhteella, tehotiheydellä ja luotettavuudella usean vuosikymmenen ajan. Koneet kuitenkin suunnitellaan edelleen jokaista toimilaitetta varten tapauskohtaisesti. Tämä työ keskittyy megawattiluokan suurnopeuskäyttöihin, joissa toimilaitteena on kompressori tai turbiini kytkettynä sähkökoneeseen. Tavoitteena on suunnitella sähkökoneen ja toimilaitteen kytkentä tavalla, joka mahdollistaa muutokset toimilaitteessa sähkökoneen pysyessä samana. Juoksupyörä asetetaan ylimääräiseen jatkoakseliin, jota tuetaan vain yhdellä radiaalisella aktiivimagneettilaakerilla. Kyseinen voimansiirto ei ole hyvin tunnettu, joten sitä on tutkittu samanaikaisesti kytkennän kanssa.

Suunnittelussa käytettävä laskenta perustuu pyörivään kappaleeseen kohdistuviin ilmiöihin kuten keskipakovoimaa, väännön välityskykyyn ja rakenteen voimatasapainoon. Käyttämällä toimilaitteen suorituskyky vaatimuksia kuten teho ja pyörimisnopeus saadaan laskettua rajoittavat arvot kytkimelle. Raja-arvoista luodaan perusmalli, josta analysointi aloitetaan. Raja-arvoja käytetään myös kaupallisten kytkinvaihtoehtojen tarkastelemiseen. Dynaamisia analyysimenetelmiä kuten roottorin kriittinen nopeus ja epätasapainon vaste on käytetty koko voimansiirron analysoimiseksi.

Työssä havaittiin analyttisten yhtälöiden avulla pystyvän luomaan perusmalliksi roottoria selvästi ohuempi liitosakseli, joka täyttää voimansiirron nopeus ja teho vaatimuksen. Kaupallisista vaihtoehdoista levykytkin osoittautui myös toimivaksi vaihtoehdoksi. Dynaamiset analyysit osoittivat, että levykytkimen avulla saadaan hieman laajempi toimialue aikaiseksi. Ohutsakselin tapauksessa voidaan siirtää myös aksiaalista voimaa. Ohutsakselin hyödyiksi löydettiin myös sen yksinkertainen rakenne ja moninaiset liitosmahdollisuudet. Työssä havaittiin myös, etteivät toimilaitteen muutokset aiheuta niin suurta vaikutusta voimansiirron käytettävyyteen uudessa kolmen laakerin ratkaisussa kuin perinteisesti käytetyssä 2 laakerin versiossa, jossa toimilaite on asennettu suoraan roottoriin.

ABSTRACT

LUT University
LUT School of Energy Systems
LUT Mechanical Engineering

Juuso Narsakka

Coupling Design and Analysis for High-Speed Drivetrain Supported by Three Active Magnetic Bearings

Master's thesis

2022

79 pages, 37 figures, 16 table and 1 appendix

Examiners: Professor Jussi Sopanen, LUT University
Professor Emil Kurvinen, University of Oulu

Keywords: High-speed electric machines, coupling design, drivetrain dynamics, rotor dynamics

High-speed machines have proved capacity to work with high efficiency, power density and reliability during many decades. However, high-speed machines are still designed case -by -case. This study focuses on megawatt range high-speed drivetrains, where a working machine is most often a compressor, or a turbine coupled with an electric machine. The target is to design coupling between electric machine and working machine in way that in the working machine can be done changes, but the electric machine stays the same. A turbine or an impeller of the working machine is placed on an additional extension shaft that is supported only by one radial active magnetic bearing. Drivetrain configuration is not well known so it's explored at the same time with the coupling.

Machine design equations based on centrifugal force, torque transfer and static equilibrium have been used in the design to calculate boundary values from the initial requirements. From the limiting values can be created a baseline model for more specific analysis. Requirements and limiting values can be also used for the comparison of the commercial coupling alternatives. Dynamic analysis methods, such as critical speed of the system and unbalance response, have been applied to the analysis of the whole drivetrain.

In the study, it was observed that with the analytical equations one was able to design solid circular shaft with specific diameter and length to match the required speed and power for the coupling. Also, from commercial couplings one was able to find a disc coupling suitable for the drivetrain. After the dynamic analysis could be seen that with the disc coupling can be obtained slightly wider operating range. Benefits of the solid shaft coupling can be found from capability to transfer axial load and wider possibilities for installation. The results also show that with three bearing drivetrain changes in impeller does not affect the usability of electric machine as much as in case of impeller attached directly on the rotor.

ACKNOWLEDGEMENTS

First, I would like to thank Jussi Sopenen and Juha Pyrhönen for allowing me to be part of their research teams during these past few years. Without their presence at LUT University, it would be impossible to study high-speed technology so top level what it is now possible.

I am thankful for Janne Heikkinen to be my director at the first steps in academic work life and Lassi Aarniovuori in the project related to this work. The most grateful I am for Tuhin Choudhury, Emil Kurvinen, and Eerik Sikanen who have been my support in my professional development during recent years. I would like to give my gratitude also for amazing teachers Kimmo Kerkkäinen, Harri Eskelinen, Olli-Pekka Hämäläinen and Timo Björk who have given me a broad basis for understanding even difficult technical matters. Without all of you this work would not be the same.

I also want to thank my family, without your support from the beginning of my life, this work would never have been done. And finally, thanks for my friends who have made the last few years so much more enjoyable.

Juuso Narsakka

Juuso Narsakka

Lappeenranta 14.4.2022

TABLE OF CONTENTS

TIIVISTELMÄ

ABSTRACT

ACKNOWLEDGEMENTS

TABLE OF CONTENTS

LIST OF SYMBOLS AND ABBREVIATIONS

1	INTRODUCTION	9
1.1	Framework and research problem.....	12
1.2	Previous research and design methods	14
1.3	Research questions.....	17
1.4	Scope of the work	17
2	COUPLING DESIGN METHOD FOR HIGH-SPEED DRIVETRAIN.....	21
2.1	Baseline values for the design	23
2.1.1	Centrifugal force	23
2.1.2	Minimum diameter for torque transmission	24
2.1.3	Static equilibrium of extension shaft configuration.....	25
2.1.4	Length for the coupling with prismatic cross-section	28
2.2	Commercial solutions available.....	29
2.3	Machine dynamic design tools	32
2.3.1	Critical speed of the system.....	33
2.3.2	Unbalance response	36
2.4	Methods for coupling's usability analysis	37
2.4.1	Effect of coupling stiffness on drivetrain dynamic behaviour.....	38
2.4.2	Commercial coupling stiffness evaluation.....	39
2.4.3	Coupling behaviour estimation in usage.....	40
3	RESULTS AND ANALYSIS	41
3.1	Requirements for the system.....	41
3.2	Baseline values for the coupling.....	42
3.2.1	Maximum and minimum values for coupling cross section	42
3.2.2	Demanded radial stiffness from static equilibrium	43
3.2.3	Baseline values as a baseline model	45
3.3	Evaluation of commercial couplings	46

3.4	Usability of couplings in three AMB drivetrain configuration.....	48
3.4.1	The effect of coupling stiffness on drivetrain dynamics.....	48
3.4.2	Disc coupling stiffness analysis.....	52
3.4.3	Usability of baseline coupling model in drivetrain.....	53
3.4.4	Usability of disc coupling in drivetrain	59
3.5	Torsional and axial natural frequencies of thin shaft and disc coupling	63
3.6	Analysing the results.....	63
4	DISCUSSION.....	65
4.1	Usability of three AMB drivetrain.....	65
4.2	Coupling in the three AMB drivetrain.....	68
4.2.1	Key findings of commercial couplings.....	70
4.2.2	Key findings of baseline couplings.....	70
4.3	In scope of future studies	71
5	CONCLUSION	73
	LIST OF REFERENCES.....	75
	APPENDIX	

Appendix I: RENK coupling stiffness analysis

LIST OF SYMBOLS AND ABBREVIATIONS

Roman symbols:

C_{\min}	minimum cap clearance
c	Distance from cross section neutral axis to the farthest surface on cross section
\mathbf{D}_M	matrix of system's damping
d	shaft diameter
E	Young's modulus
F	Force
F_a	Amplification factor
F_r	radial force
$\mathbf{F}(t)$	vector of forces in system
F_u	Force due to unbalance
F_y	Unbalance force in radial y direction
F_z	Unbalance force in radial z direction
f_{dyn}	dynamic factor
G_i	ISO 21940 unbalance G- grade
\mathbf{G}_M	matrix of gyroscopic effects
g	Gravitational acceleration
I	second moment of area
\mathbf{K}	matrix of system's stiffness
K_f	Stress concentration factor for bending
K_{fs}	Stress concentration factor for torsion
k_r	radial stiffness
L	length of the beam
\mathbf{M}	matrix of system's moments of inertia
M	Moment
M_a	alternating bending moments
M_m	midrange bending moments
M_{s1}	separation margin, operation speed is higher than resonance frequency
M_{s2}	separation margin, operation speed is lower than resonance frequency

m_r	mass of part where unbalance is located
m_s	shaft mass
m_u	mass of unbalance
n	Safety factor
n_c	frequency of resonance
n_l	frequencies in right side of resonance
n_u	frequencies in left side of resonance
P	Power
$q(t)$	displacement of reviewed point in the system
$\dot{q}(t)$	velocity of reviewed point in the system
$\ddot{q}(t)$	acceleration of reviewed point in the system
r_e	outer radius of ring, cross section
r_i	inner radius of ring, hollow cylindrical cross section
r_u	radius of the unbalance location
S_e	reduced strength of material
S_{ut}	ultimate tensile strength
T	Torque
T_a	Alternating torsion moment
T_m	midrange torsion moment
t	time
U	effective unbalance
x_1	distance between center of shaft mass and center of AMB location
x_2	distance between AMB location and impeller's center of mass
x_3	distance between coupling support location and AMB
y	distance from the center of disc to position of interest

Greek symbols:

α	initial angular position of the unbalance mass
δ	Deflection of the beam
δ_{max}	maximum radial displacement
ρ	density of the material
σ_a	bending stress from alternating load

σ_b	bending stress
σ_m	bending stress from midrange load
σ_{\max}	total stress in calculation location
σ_r	radial inertia stress
σ_θ	tangential inertia stress
τ_a	Torsion stress from alternating load
τ_m	Torsion stress from midrange load
ν	Poisson constant
Ω	Angular velocity

Abbreviations:

AMB	Active magnet bearing
BW	Backward whirling
DHS	Direct high-speed
FEA	Finite Element Analysis
FEM	Finite Element Method
FW	Forward whirling
HSEM	High-speed electric motor
RoBeDyn	Rotor-Bearing Dynamics
S355	Structural steel, 355 MPa tensile strength
S700	Structural steel, 700 MPa tensile strength

1 INTRODUCTION

This study is motivated by the need to find out whether it is possible to produce a megawatt-class high-speed electrical machine drive so that the same electrical machine can be used in a various application. The most important high-speed applications have for a long time been turbines and compressors (Pyrhönen et al. 2009 pp. 35 – 36). Pressurising of natural gas is one example of a high-speed application which uses a gas turbine to rotate the compressor impellers creating pressure difference to transfer the gas in the network. To reduce carbon dioxide emissions gas turbine can be replaced with a high-speed electric motor (HSEM). (Gilon & Boutriau 1998 p.1.)

As another example, heat pumps can be mentioned as one solution to replace natural gas usage in heating purposes. The heat pumps can transfer thermal energy between two spaces by compressing the circulating fluid (refrigerant) in a closed circuit between the spaces. Refrigerant is charged with thermal energy at low pressure and discharged under high pressure and temperature. The mechanical energy needed for energy transfer is typically 20 – 30% from the total heat energy. If mechanical energy is produced by an electric motor and electricity comes from a renewable energy source, process can achieve significant emission reductions compared to the burning fuels. (Zhang et al. 2016, pp.801 – 808.)

The above-mentioned combination with an electric motor or a gas turbine (driving machine) and a compressor (driven machine) is called a drivetrain (Feehally 2012, p.25). The most used system to produce a high speed for an impeller (actuator in a compressor) is a standard-speed electric motor coupled to a step-up gearbox that is coupled to a stand-alone high-speed compressor (compressor is equipped with its own shaft, bearings, and frame) (Global Industry Analysts Inc 2020). Figure 1 shows an example of a geared drivetrain where the application is a vacuum compressor (left) and the actuator in it is a single-stage radial-outflow impeller driven by electric machine (right) and between is a gearbox.

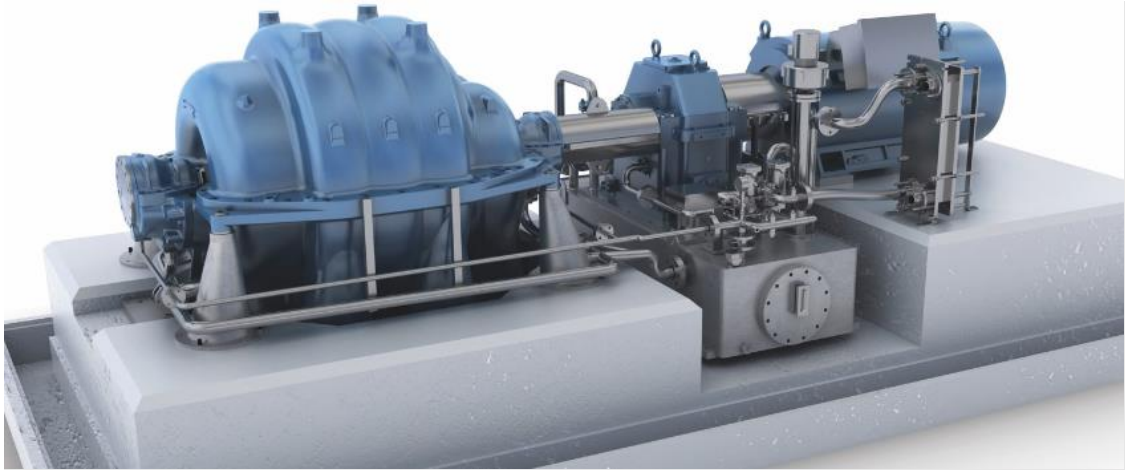


Figure 1. TURBAIR vacuum blower drivetrain. From left; radial vacuum compressor, coupling, gearbox, coupling, electric motor. Below the gear oil reservoir for the gear lubrication. (MAN Energy Solutions 2021).

The annual sales volume of high-speed drivetrain in megawatt power range can be measured in billions. So far, direct high-speed (DHS) solutions account for only about 5% of the annual sales in megawatt range. (Global Industry Analysts Inc 2020.) A DHS solution refers to drivetrain without gearbox where both motor and application can stand on with own bearings or as an integrated solution like previously mentioned turbine-compressor solution or a high-speed electric motor-compressor drivetrain when an impeller is attached directly on HSEM's shaft (rotor) (Pyrhönen et al. 2009, p.35; The Switch 2021.) Figure 2 shows the same application in use than Figure 1 but with DHS configuration.

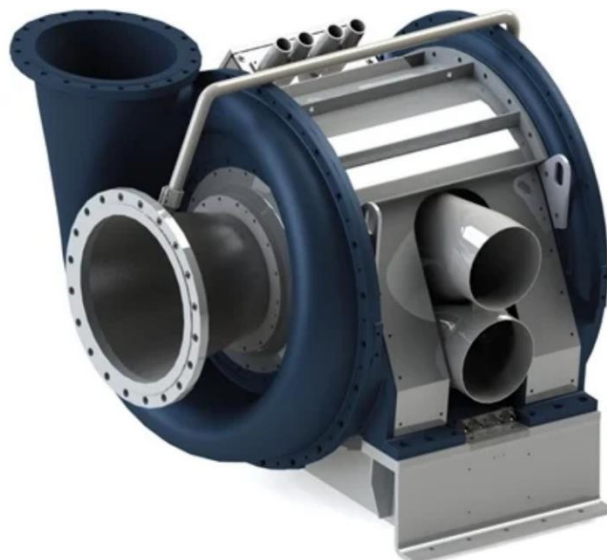


Figure 2. RunEco Turbo blower (vacuum). Impeller is attached directly on electric motor's rotor. (Gardner Denver 2021).

It is difficult to evaluate precisely, why the DHS market share is so small in megawatt range. One possible cause can be relatively long product development times of DHS machines. Especially in the case of integrated solutions, custom design is required case -by -case basis (Kurvinen et al. 2021a p.1). Due to long development period the first machine price is high. The price would be able to reduce by producing larger volumes at once. Over megawatts class machine volumes per similar function are often only a few units (Gilon & Boutriau 1998 p.4). Thus, design is easily carried out with a solution in which the e.g., compressor is designed as a stand-alone solution that can be attached to a standard gearbox drivetrain. Therefore, only the compressor needs to be designed on a case -by -case basis.

In the case of DHS use, the challenge is to adapt electrical, thermodynamical, mechanical, and fluid dynamical optimal solutions in the same frame while the manufacturability needs to be guaranteed. Changes in one part of DHS machine may affect other components critically. Therefore, it is difficult to avoid multidisciplinary design when a well-functioning result is aimed at. The advantages of DHS drives are a system compact size that saves materials and reduces the number of parts. DHS removes the need for the continuous maintenance of the gearbox and reduces the need of the lubricant. (Gilon & Boutriau 1998 p.1; Kurvinen et al. 2021a, pp.1-2.) In some applications like Organic Rankine Cycle the hermetic structure offers benefits due to closed loop system (Access-energy 2022). The integrated DHS drivetrain avoids the need of shaft seals, which are problematic for proper seal design (Kleynhans et al. 2005 p.65).

Full benefit of a DHS drive is obtained when an active magnet bearing (AMB) is introduced in the system. With AMBs the drivetrain does not need continuous maintenance and lubricants in its entirety. This enables to build a drivetrain that is an economically (operating costs) and environmentally better solution. (Gilon & Boutriau 1998 p.2; Kurvinen et al. 2021a, p.1.) To remove the disadvantages of DHS drives, the challenges of the acquisition of the machine must be solved. If HSEM could be produced in serial production in the same way as standard electric motors, it would give a huge usability improvement for DHS drives.

1.1 Framework and research problem

During the last five years, the possibility of serial produced megawatt range HSEM design has been studied actively at LUT University. Innovation of research is a solution that combines the positive sides of the geared and DHS drivetrain. The solution is a drivetrain in which the electric machine stays the same and when necessary, it is equipped with an extension shaft including a third AMB. With this modular structure only the extension shaft will be designed case-by-case. The purpose of the third bearing is to carry loads caused by an impeller or impellers. Thus, the bearings of the electric machine do not need changes as a result of changes in impeller. The HSEM can be designed to work with lower-level impeller loads and with stand-alone machines. When direct integration of an impeller leads to a supercritical design the third bearing can be taken in use. The deployment of the method requires that the rotor dynamics of the electric machine will not significantly change when the three-bearing configuration is applied. Figure 3 illustrates the DHS drivetrain, stand-alone drivetrain, and three-AMB-two-shaft drivetrain, where the red rectangles illustrate bearing positions. Kleynhans et al. (2005) presents these drivetrain configurations in natural gas compression application, with an exception that the three-bearing solution is designed from a single shaft.

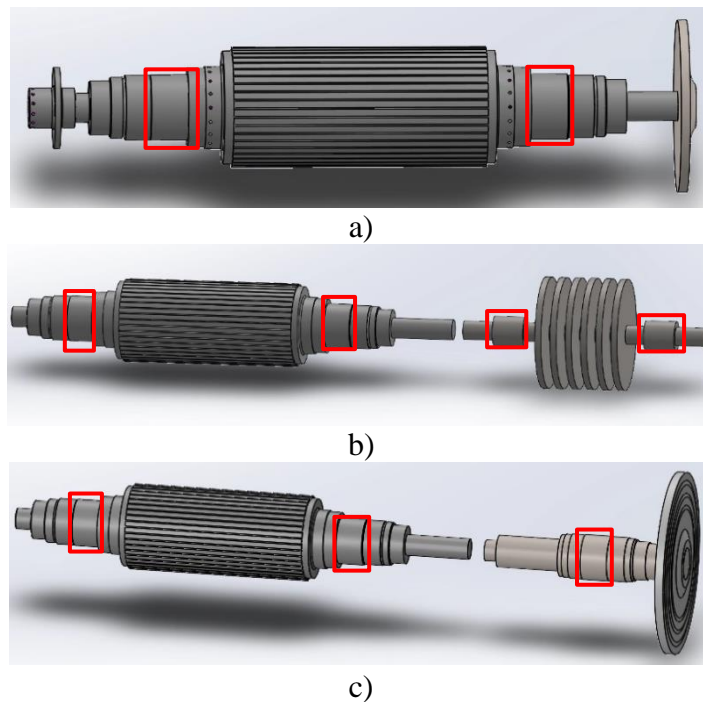


Figure 3. Three different HSEM drivetrain configurations. a) Impeller is attached on the electric motor shaft (DHS drivetrain). b) Impellers are supported with own bearings (stand-alone drivetrain). c) Impeller is installed on extension shaft, (three AMB drivetrain). Red boxes indicate the locations of the bearings.

Stand-alone compressors are commonly used with flexible couplings. The main purpose of the coupling is to allow misalignment that cannot be avoided in practical conditions. The flexibility of the coupling has also been found to have a positive effect when designing the dynamics of the machine. (Zhao et al. 2016, p.207.) High-speed machines are often defined according to have circumferential speed in the range of (60 – 370 m/s). Machines which operate at such high speeds behave as a flexible body. This means that the rotor vibrates not as a one straight body (rigid) but curved in shape against its rotational axis i.e., rotor is bending. (Gerada et al. 2014, pp. 1-8.) Other machine parts can vibrate as well in a flexible mode which must be considered e.g., in the frame design.

When the rotor behaves as a flexible body, changes in geometry significantly affect its vibration response. (Kurvinen et al. 2021b p.7.) Thus, when the rotor is coupled to another part such as an impeller or shaft, machine vibration behaviour may change so much that it is not usable anymore. On another hand, four bearing drivetrains are used with flexible couplings. Thus, the initial hypothesis of the study is set as:

- By creating a flexible coupling between the rotor and the extension shaft, attachment of the third AMB and impeller does not affect the electric machine so much that structural changes must be made in it.

The problem with the hypothesis is that even if it were true, it is not known whether the coupling can be implemented to meet requirements like stresses from high velocity, stability, inner and external forces etc. Couplings have been studied for a long time. However, the three active magnetic bearings configuration under the study is one of the kinds and for that reason there is not direct information for the case. From literature one can find information of one shaft three bearing solution, four bearing systems and different coupling possibilities in markets. (Kleynhans et al. 2005; Srinivas et al. 2018, p.538 – 571; Tollok 2003; ISO 10441.)

When drivetrains are designed the coupling design is more like a coupling selection. Manufacturers offer products in certain operation parameter ranges and customer needs to find right one to match with requirements. On the other hand, researchers study a very

narrow section at the time, and it could be hard to use those results in a design process straightforwardly. The current design methods for coupling focus in fulfilling the requirements like torque transfer capacity and misalignment capacity. Clear design processes and methods are not presented well for coupling design in special cases. (Tollok 2003; Fenner drives 2012; Norelem 2021; Norton 2006, p.559 – 562; ISO 10441.)

The difficulty of the three AMB drivetrain coupling design may lie in usage of static or steady state values in analysis. In a three AMB solution with various speed usages those can result in under or over design. Dynamic analysis is needed for better understanding of requirements of the coupling. Dynamic analysis always needs a model to be analysed. Model can be based on calculations called as baseline model or it can be just a sketch of feeling (based on experience) (Kurvinen et.al 2021b, pp.4-7).

Zhao et al. (2016) present that a flexible coupling needs to be stiff in radial direction. So, the biggest contribution in the design may occur in the balance of the load capacity in nominal and overload situation to the flexibility of the coupling. In overhung situation the impeller is supported with the coupling and the third bearing. The flexibility of coupling hypothetically enables using the same HSEM with different impellers but does that flexibility ensure reliable usage against forces over the coupling.

Using the overhung with pivot point structure it is uncertain how much unbalance and misalignment correlate with each other. Impeller unbalance creates a force to the coupling which leads to some deviation in displacement. That will increase the angular misalignment in the system which can excite higher vibration levels. Correlation problem and how to control it with AMB supported drivetrain can be solved only with AMB control design.

1.2 Previous research and design methods

Previous research related to this work can be divided into four categories: effect of coupling stiffness, design requirements for high-speed coupling, mechanical engineering design and AMB systems. Stiffness in mechanical engineering is a long-studied topic. Rivin (1999) has written a book which focuses in clarifying how stiffness and damping characteristics can be used in design parameters.

Lee et al. (2019) have published an article of varying-stiffness flexible coupling. They studied a magnetorheological flexible coupling. It can tune the flexibility of coupling's magnetorheological elastomer by controlling its external magnetic field. They managed to adaptively tune resonance frequencies between 16.8 and 23.5 Hz. The purpose of the study was to develop a coupling which could avoid torsional natural frequencies of a gearbox by tuning the stiffness during the usage. (Lee et al. 2019, p.1.)

Zhao et al. (2016) have compared Finite Element Analysis (FEA) and experimental results of a flexible disc coupling under varying torsional load. They have concluded that torsional stiffness in a flexible disc coupling is nonlinear as a function of torque. Corcoran et al. (2007) present a study of advances in gas turbine coupling. Rotordynamics related to coupling is discussed and they are presenting an example of coupling's support stiffness in relation of its critical speed. (Zhao et al. 2016, p.207; Corcoran et al. 2007, pp.168 – 170.)

In the field of design requirements Locke et al. (2013) has published a study of coupling credible failure modes and how to intervene them. They listed the most important design information for special purpose couplings. A special purpose coupling can be considered when the operation of the plant depends on the operation of the coupling and requires a high-power transfer or rotational speed. The text mentions the following: "-- 12 000 RPM compressor is certainly special purpose and critical to trouble free operation". (Locke et al. 2013.)

Standards are widely used in mechanical engineering to set requirements and guidelines for the design. API 671 / ISO 10441 the standard specifies guidelines for the operation of flexible couplings in petroleum, petrochemical, and natural gas industries in special purpose applications. The standard applies to gear, metallicly flexible elements, quill shafts and torsionally resilient type couplings. Standard presents also overall design process for coupling selection. (ISO 10441, pp.1-8.)

Machine design is naturally a field that has been studied for a long time. Pahl and Beitz (1996) go through a systematic approach in their book Engineering Design. A systematic design process can be divided into four main steps which are clarification of the task, conceptual design, embodiment design and detail design. (Pahl & Beitz, 1996, pp.67–70.)

Chen and Zeng (2006) present different theories to address design requirements from machine's every lifecycle step in their research. Kurvinen et al. (2021b) presents a design space method for conceptual design exploration in the field of high-speed electric machines. The study shows how initial requirements can be utilized for baseline model creation and optimization of it. (Chen & Zeng 2006, pp.220 – 223; Kurvinen et al. 2021b.)

Machine design books present calculation methods for machine element design. Calculations for commonly used machine element like bearings, gears, shaft, screws, etc. can be straightforwardly utilized from literature. (Burdynas & Nisbett 2015; Norton 2006.) Birolini (2007) brings forth the reliability base design in his book Reliability Engineering. Eskelinen and Karsikas (2013) have studied Design for Manufacturing and Assembly which underline the importance of simultaneous identification of suitable manufacturing methods for the design. (Birolini 2007; Eskelinen 2012.)

Wayzode & Tupkar (2012) have studied how 3D modelling can be accelerated by calculating the baseline values with analytical equations and entering the data for 3D software by using Macros. Burdynas and Nisbett (2015) have studied computational efficiency between beam and solid element model in their book. They are presenting difference in two section non-prismatic shaft structure. Difference of first two natural frequency was reported to be less than 4% when using solid and beam elements. (Burdynas & Nisbett 2015, pp. 964-965; Wayzode & Tupkar 2012, pp.30-32.)

Srinivas et al. (2018) have published extensive research of applications of active magnetic bearings in flexible rotordynamic system. It has noted over a hundred AMB research papers and tens of different AMB drive configurations. In three different papers a three-radial-AMB system was reported. Configurations of drives were not presented in the paper and original publications were not in free access. The text suggests that the systems were constructed so that the third bearing was either an excitatory or a damper in the system which means that it did not work as a support for shaft. (Srinivas et al. 2018, pp.538 – 571.)

1.3 Research questions

From the previous research a similar three-AMB structure as presented earlier in the introduction (Figure 3 c) was not found. The stiffness of the coupling can clearly be said to have an effect on system dynamic response, but a clear picture to confirm the hypothesis does not emerge from previous studies. As this is a new solution, clear instructions for a novel coupling design cannot be found directly from the standards, literature or by the coupling manufacturers.

The aim of this study is to develop a method for solving the hypothesis of flexibility and then design a concept level solution for the coupling. The results should be obtained at a level that can be utilized in AMB control design and testing of the control algorithm. Consequently, it is essential to produce not only the most potential options for the coupling but also rapid methods for design for possible subsequent changes. Thus, the key research questions have been set as:

1. What design tools are needed and how the design is managed in a reliable and efficient way?
2. Why stiffness of the coupling is important or is it?
3. What are the limiting and most optimal coupling parameters with the three-AMB configuration?
4. How the result can be utilized in further studies?

1.4 Scope of the work

The scope of the work is set around a previous study at LUT university. The case study in this work is a coupling between a multimegawatt HSEM and an extension shaft (Figure 3). The electrical motor is an induction motor with a solid slitted rotor supported by AMBs. The machine is designed to reach 1670 Nm torque at 12,000 rpm resulting in 2 MW power. (Kurvinen et al. 2021a, p.5). The rotor drive end is equipped with two AMB locations for research reasons. However, a similar commercial rotor would be made with only one bearing per end. Thus, the rotor configuration has been updated into a two AMB system. Figure 4. a) illustrates the case study rotor and Figure 4. B) its dimensions.

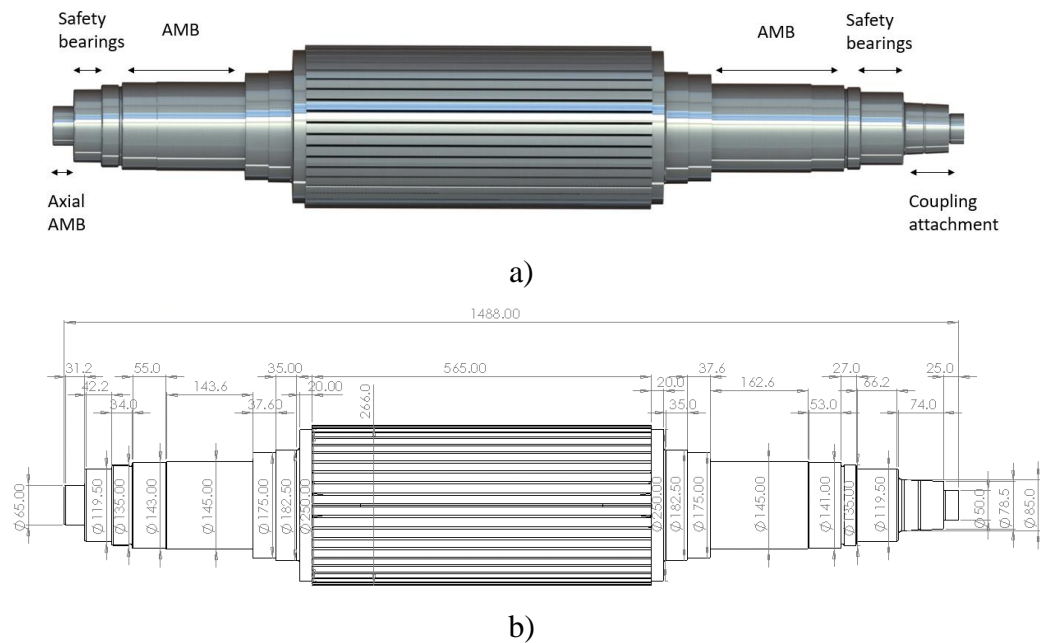


Figure 4. a) Case study rotor. b) Dimensions of rotor.

The extension shaft is designed parallel with this study. Some changes to the extension shaft may occur during the coupling design. The impeller in the case study is a turbine wheel from a hermetic high-speed turbogenerator concept for biomass and waste heat recovery studied in LUT. It must be noted that the preliminary extension shaft configuration is not designed to work in turbine configuration where the turbine disc is originally used. The turbine is designed to produce 1 MW mechanical power at 12480 rpm. (Grönman et al. 2020.) Designed power for turbine wheel is from lower end of the electric machine's designed power range. Although the turbine wheel is not matching perfectly for the machine power range, more important is to study how the drivetrain behaves. To draw conclusions from the results of this study, it is good to have a reliable benchmark case. Previous research work with the same turbine, which also has experimental results, is therefore excellent for this purpose. The baseline model for the extension shaft is presented in Figure 5 and its dimensions in Figure 6. Turbine wheel blades are suppressed in the analysis from the model for better computational efficiency.

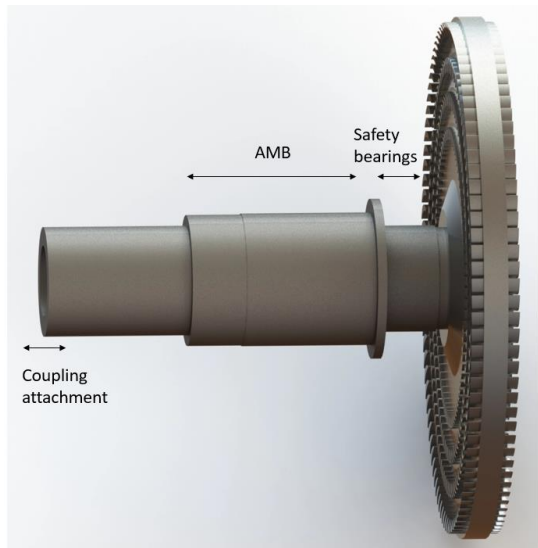


Figure 5. Baseline model of the case study extension shaft and the turbine wheel.

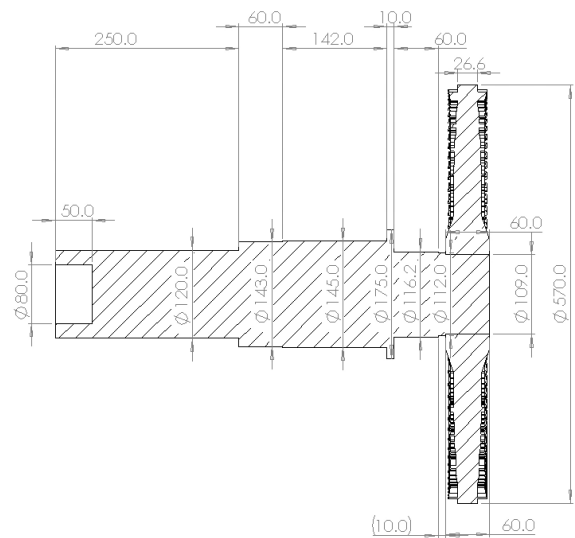


Figure 6. Dimensions of the extension shaft configuration

Figure 5 and Figure 6 do not present the AMB lamination stack on the shaft. Lamination outer diameter is 175 mm. When the lamination is included the analysis for it has been used same material properties than for extension shaft. Material properties of the case study parts are presented in *Table 1*.

Table 1. Calculation parameters of case study drivetrain. (Grönman et al. 2020; Jin et al. 2016 pp.6–7; Kurvinen et al. 2021a, p.5.)

Parameter	Unit	Value
Disc density	kg/m ³	4820
Disc Elastic Modulus	GPa	104
Disc Poisson's Ratio		0.33
Disc mass	kg	41
Disc Moments of Inertia: x / y, z	kgm ²	1.64 / 0.82
Rotor / Extension shaft density	kg/m ³	7800
Rotor / Extension Elastic Modulus	GPa	210
Rotor / Extension Poisson's Ratio		0.29
Extension shaft mass	kg	66.6
Rotor mass	kg	331
Equivalent support stiffness of AMB	N/m	4·10 ⁶
Equivalent support damping of AMB	Ns/m	2·10 ³

As mentioned earlier, the AMB control algorithm should be developed based on the existing model. The development of the model requires special expertise and is, therefore, out of scope in this work. On the other hand, the results of AMB simulation are needed to make the final coupling design decision. For this reason, the design process cannot be completed, and the study focuses more on the development of a conceptual design method for a three-AMB drivetrain and set the boundary conditions for coupling based on initial requirements.

Chen and Zeng (2006) present eight requirement priority levels. The idea of levels is to categorize which requirements designers can or cannot affect in the design. The highest level includes natural laws and rules. The study focuses in matching initial requirements to natural laws. Other requirements for design, like manufacturing and sale, are kept in mind but are not studied in detail and are not reported in this work. Material selection is carried out with very basic engineering materials used in previous studies.

Because of the scope of this work, expected results are not the final design but a preliminary model for further analysis. The more important results are knowledge of stiffness properties demanded by the coupling. Which commercial couplings can be utilized and is there a need for a totally new coupling? Another important result is a design procedure to be utilized in another case in the future. If the hypothesis will be proven to be correct, and the coupling can be designed to fulfil the other requirements (e.g., stability), the effect of the work can be significant in the future in the field of high-speed applications by helping the DHS manufacturers for easier utilization of their machines.

2 COUPLING DESIGN METHOD FOR HIGH-SPEED DRIVETRAIN

Due to the specificity of the design work, the design process does not fit directly to any specific method. However, the design is, in big picture, part of a systematic design process which can be divided in four main steps: clarification of the task, conceptual design, embodiment design and detail design. (Pahl & Beitz 1996.) Obtaining requirements for the design is a key part of the conceptual design phase. Chen and Zeng (2006) present different theories to address requirements of the design in their research. One of the theorems is the source of product requirements, which aims to collect requirements from every aspect of the product life cycle. The product life cycle segments are divided into seven categories which are; Design, manufacture, sale, transportation, use, maintenance, and recycling. As can be seen, a wide variety of requirements must be considered in a design. Not all requirements can be implemented in the best possible way. To understand what the key requirements are, it is necessary to categorize them in different priority levels. Chen and Zeng use an eight-level division where the lowest level contains the most important requirements. Figure 7 illustrates the eight-level division. (Chen & Zeng 2006, p.224.)

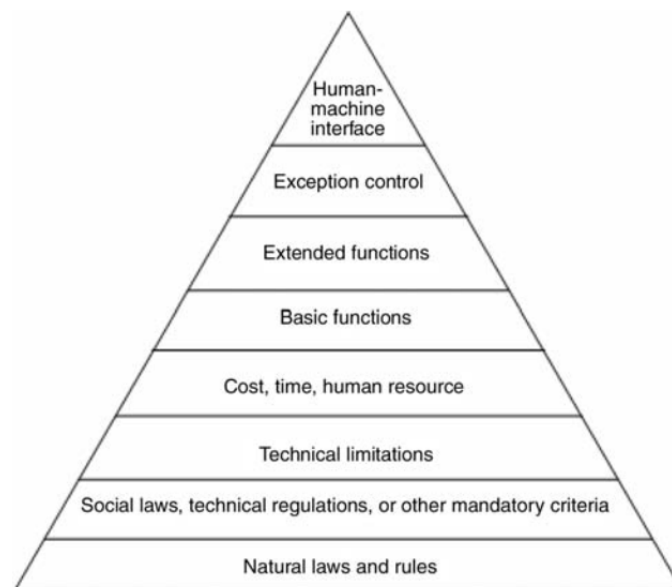


Figure 7. Machine design priority levels according to Chen & Zeng (2006)

Those eight levels can be classified non-functional requirements (four lowest), and functional requirement (top four). Non-functional requirements are most often requirements

where a designer cannot affect directly. A product offered in a certain region must follow its social laws and regulations. (Chen & Zeng 2006, p.225.) For example, the frequency of the power grid changes between regions. The time spent in designing a product can be very relevant to its competitiveness. Rapidly evolving products become quickly obsolete as new technologies enter the market. Technical limitations can be seen e.g., in the field of manufacture or process environment where old systems do not support new technologies. The highest boundaries of all the requirements come from natural laws and rules. Those rules cannot be overridden but, on the other hand, design practices can heavily lean on them. For example, in rotating ring stresses of the part is proportional to the square of the angular velocity (Budynas & Nisbett 2015, p.129).

When requirements for the design are decided (e.g., in HSEM design power and speed) systematic design process is started by brainstorming ideas. However, in a clearly defined function, it is possible to start by calculating a baseline model based on the requirements as presented in paper by Kurvinen et al. (2021b). The above-mentioned design methods can be combined to execute effective design for case study coupling. Figure 8 presents the flowchart of the design process.

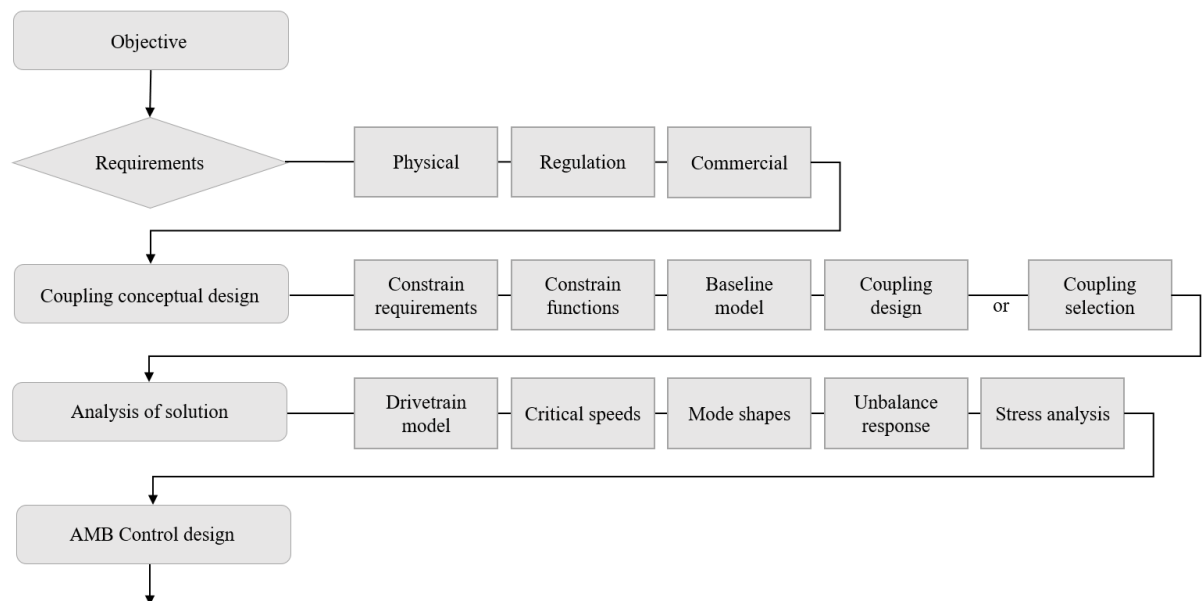


Figure 8. Flowchart of the design process for the case study coupling.

Regulation and Commercial requirements are kept in minor part but used in contexts as safety, manufacturable and cost-efficient product. Expressed at its simplest the requirement for the coupling comes from the target to transfer mechanical power. Power (P) can be calculated from angular velocity (Ω) and torque (T) applied in the coupling.

$$P = T\Omega \quad (1)$$

The main requirements of the design are thus formed according to the torque and speed. Those parameters make it possible to form equations based on the natural laws. Equations can be used to solve the minimum or maximum mechanical requirements (baseline values). These baseline values can be used to evaluate existing solutions and to develop new ones. Baseline data rarely provide the best possible solution or even a usable solution. However physical solution is needed for dynamic analysis because dynamic behavior depends on the geometry, material, attachment etc. parameters of the part.

Next sub-chapters introduce the coupling conceptual design (2.1 Baseline values for the design, 2.2 Commercial solutions available), and analysis of solutions (2.3.1 Critical speed of the system, 2.3.2 Unbalance response) regarding Figure 8 flowchart.

2.1 Baseline values for the design

Baseline values are calculated according to static situation. A dynamic factor can be used to tune results closer the real situation. Active magnet bearing design where the bearing is dimensioned according to the static situation, the dynamic factor for load capacity is typically selected as 5 – 7 to static load (Kurvinen et al. 2021a). Modelling and analysing a dynamic situations takes considerably more time than analysing a static situation. Therefore, in the design of the concept level, it is desirable and justified to use simplified models and methods. Detailed dynamic simulations should be performed at later stages of the design.

2.1.1 Centrifugal force

The first limiting value for the design can be calculated from the rotational speed of the part. The maximum diameter of the rotating part is restricted by centrifugal force. As the part rotates, its particles are subjected to centripetal acceleration which creates an inertia-dependent force on the part, leading to internal stresses. For a disc-shaped part ($r > 10 \times \text{disc}$

thickness, two-dimensional plane stress assumption), the radial and tangential stresses can be calculated by the following formulas:

$$\sigma_r = \left(\frac{3+v}{8}\right) \rho \Omega^2 \left(r_i^2 + r_e^2 - \frac{r_i^2 r_e^2}{y^2} - y^2 \right) \quad (2)$$

$$\sigma_\theta = \left(\frac{3+v}{8}\right) \rho \Omega^2 \left(r_i^2 + r_e^2 + \frac{r_i^2 r_e^2}{y^2} - \left(\frac{1+3v}{3+v}\right) y^2 \right) \quad (3)$$

Where σ_r is radial inertia stress, σ_θ is tangential inertia stress, v is Poisson constant, ρ is density of the material, r_e is outer radius of ring, r_i is inner radius of ring and y is distance from the center of disc to position of interest. (Budynas & Nisbett 2015, p.129.)

2.1.2 Minimum diameter for torque transmission

For the load capacity, baseline values can be calculated from shaft design calculations. In the shaft design it is important to consider all possible load situations. In addition to torsion, the shaft may be subjected to bending, normal force and radial and longitudinal shear. In most cases the normal (axial) load and radial & longitudinal shear are excluded from calculation because those are usually in minor role in critical locations. When geometry determination is in its final step all loads can be applied in the analysis. (Locke et al. 2013; Budynas & Nisbett 2015, pp.358-360.)

For the shaft design calculations loads are considered as fluctuating loads. With fluctuating loads stresses cannot be compared straight to the tensile strength of the material. Many theories have been developed for fatigue analysis. Modified Goodman theorem is one of the commonly used theorems with ductile materials. Stresses affect also in same locations but in different directions. Distortion energy failure theory (Von Mises stress theory) can be added to combine the stresses in the same location. Combining the Modified Goodman and Von Mises stresses minimum shaft diameter (d) for full circular profile and infinite lifespan can be calculated as:

$$d = \sqrt[3]{\frac{16n}{\pi} \left\{ \frac{1}{S_e} \sqrt{4(K_f M_a)^2 + 3(K_{fs} T_a)^2} + \frac{1}{S_{ut}} \sqrt{4(K_f M_m)^2 + 3(K_{fs} T_m)^2} \right\}} \quad (4)$$

Where n is safety factor for fatigue, S_e is reduced strength (Ultimate tensile strength multiplied with factor depending on the load type etc.), S_{ut} is ultimate tensile strength, K_f is stress concentration factor for bending, $M_{a/m}$ are alternating/midrange bending moments, K_{fs} is stress concentration factor for torsion and $T_{a/m}$ are alternating/midrange torsion moment. (Budynas & Nisbett 2015, p.237, 311, 360.) For precise S_e is needed material, geometry, operating temperature, reliability level and manufacturing details. The dominant load type also affects reduction. With a new design that information may not be known in early design. From the machine design books can be found pre-calculated values for common designs. (Budynas & Nisbett 2015, pp.227-357.)

In case of high steady torsional stress with low alternating bending load (or safety factor for infinite lifespan is below 1) equation 4 does not include yield of the material. Yielding can be analysed with Von Mises stress theory as:

$$\sigma_{\max} = \sqrt{(\sigma_a + \sigma_m)^2 + 3(\tau_a + \tau_m)^2} \quad (5)$$

Where σ_{\max} is total stress in calculation location, $\sigma_{a/m}$ are bending stress from alternating and midrange load and $\tau_{a/m}$ is respectively from torsion. (Budynas & Nisbett 2015, p.362.)

2.1.3 Static equilibrium of extension shaft configuration

In ideal four bearing drivetrain coupling does not transfer anything else than torque with constant speed or acceleration around of rotating plane. However, there is always some deviation in the system, which leads to forces affecting also other planes. In the case study drivetrain has supported only one bearing on impeller side. It means that the coupling acts as second support location for the overhung load (Figure 9). Because of flexibility of any material force generates a displacement in the coupling. Maximum displacement can be analyzed more precisely with further simulations. An estimation for initial calculation can be made from the vibration limits. Limits for over 15 kW AMB machines are determined in ISO 14839-2 (2004) standard. With a new machine vibration measured from AMB location can be at maximum 0.3 multiplied minimum cap clearance (C_{\min}) between the shaft and the safety bearing. (ISO 14839-2 2004, p. 7.)

For static calculations it is not reasonable to utilize the dynamic situation limits straightforwardly. With AMB design static calculations are performed and dynamic force estimation is found by multiplying the static force with dynamic factor (f_{dyn}). The same method can be utilized with coupling support force analysis. So, maximum radial displacement (δ_{max}) can be presented as:

$$\delta_{max} = \frac{0.3C_{min}}{f_{dyn}} \quad (6)$$

The necessary radial stiffness (k_r) can be calculated from spring rate equation:

$$k_r = \frac{F_r}{\delta_{max}} \quad (7)$$

when maximum radial force (F_r) and radial displacement is known. (Norton 2006, p.739.) The force can be calculated from static equilibrium of drivetrain configuration. Forces affecting the system are reduced to consider only the extension shaft side. Electric machine rotor is considered a rigid support. Figure 9 illustrates the free body diagram of drivetrain where blue arrows are support forces and red arrows loads.

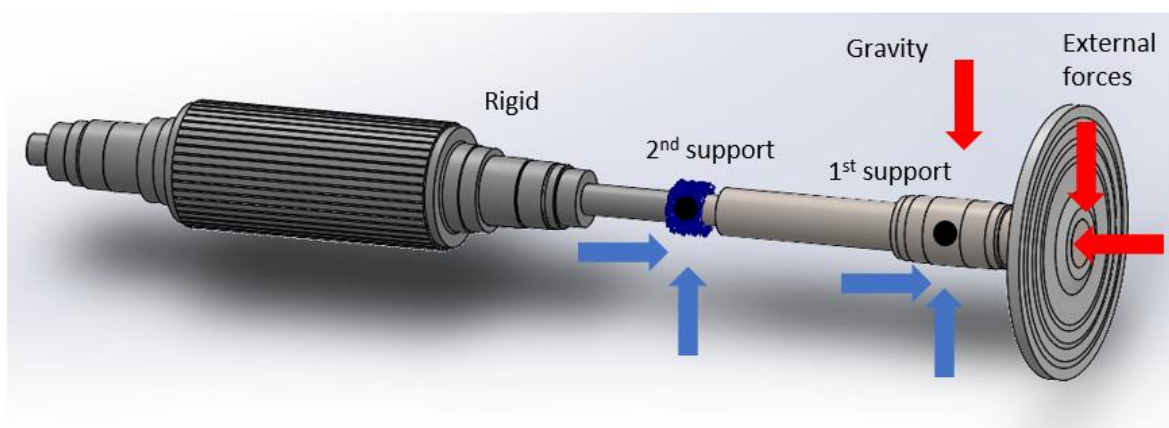


Figure 9. Free body diagram of the drivetrain to calculate the 2nd support location radial support force.

External forces depend on impeller in use. In this phase of design external forces are excluded from calculations. Dynamic behaviour can be taken into consideration by adapting the unbalance force. Force due to unbalance (F_u) can be calculated as:

$$F_u = m_u r_u \Omega^2 \quad (8)$$

Where m_u is mass of unbalance and r_u is radius of the unbalance location. After manufacturing all parts have some unbalance. Unbalance forces can be distributed all over the part in small fractions. In that reason, all high-speed machines are balanced after manufacturing to avoid uncontrollable vibration. After the balancing machines include still a residual unbalance. ISO 21940 standard uses G value determination, which informs maximum velocity of vibration. A part balanced according to category 2.5 G means that in operation speed maximum vibration can be 2.5 mm/s. With G grades effective unbalance (U) can be calculated as:

$$U = \frac{G_i m_r}{\Omega} = m_u r_u \quad (9)$$

Where G_i is G- grade in m/s and m_r is mass of part. (ISO 21940-11 2017.) Design can be started with maximum residual unbalance in commissioning stage. However, coupling and drivetrain need to operate in long term when unbalance may increase in different locations. Sensitivity analysis can be made to estimate how much unbalance affects coupling support force.

By adding the parts own mass effectiveness, the total radial force (F_r) can be calculated from the static moment equation around the AMB location as:

$$F_r = \frac{m_s g x_1 + m_a g x_2 + F_u x_2}{x_3} \quad (10)$$

Where m_s is shaft mass, x_1 is distance between center of shaft mass and centre of AMB location, m_a is mass of the impeller, x_2 is distance between AMB location and impeller's centre of mass. x_3 is distance between coupling support location and AMB. g is the gravitational acceleration ($\frac{m}{s^2}$). Inserting equation (7) into the equation (10) the required stiffness can be calculated.

2.1.4 Length for the coupling with prismatic cross-section

The baseline diameter of circular profile was calculated based on transmitted torque. The baseline length of the coupling can be calculated with beam deflection by utilizing the required radial stiffness. Beam deflection with different constraints can be found from literature. The theoretical case and the real situation may not match precisely for each other, the usability of the equations can be analysed with FEA and verified with experimental results. If the coupling is considered as rigidly attached from rotor end and into the other end is added radial force, model can be presented as Figure 10 shows. The use of the equation requires that the mounting is considerably stiffer than the coupling, i.e., the rotor and the extension shaft must be considerably larger in diameter and the attachment must be as rigid as possible.

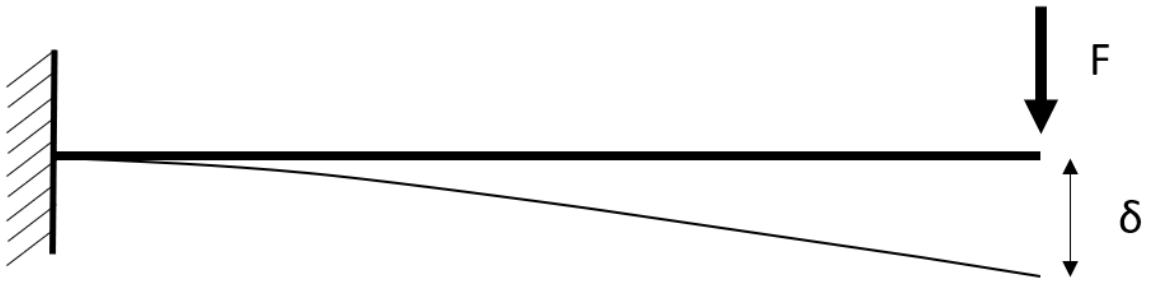


Figure 10. Applied beam case to solve the maximum length of the coupling.

Deflection of the beam (δ) can be calculated in Figure 10 case as:

$$\delta = \frac{FL^3}{3EI} \quad (11)$$

Where F is applied force, L is length of the beam, E is Young's modulus and I is the second moment of area. (Budynas & Nisbett 2015, p.359, 1021.) Relation between force and deflection can be present with spring rate equation, when beam is circular in shape equation for length can be present as:

$$L = \sqrt[3]{\frac{3E\frac{\pi}{4}(r_e^4 - r_i^4)}{k_r}} \quad (12)$$

Where r_e is outer radius and r_i is inner radius of hollow cylindrical cross section.

2.2 Commercial solutions available

In general, couplings can be divided into two categories, rigid couplings and compliant couplings. The difference between those categories is the capability of compliant couplings to handle the misalignment between two shafts. Typical rigid couplings are setscrew, keyed, spline and clamp couplings. Setscrew and keyed couplings transfer torque through screw, pin, or key. Ends of the shaft are inserted almost face to face and coupling body (bushing) comes over the shafts. Bushing can be tightened over the shaft when friction between the shaft and the bushing transfer portion of the torque. Spline coupling works with the same principle as a key but in a spline coupling case bushing and shaft's end are machined like gears and fitted over each other. A clamp coupling differs from others so that it transfers torque only with friction between the shaft and the coupling. (Norton 2006, p.559.) Friction can be generated e.g., by shrink fitting. This type of attachment is called interference fit (Childs 2014, p.767). Figure 11 shows a section view of a keyed coupling and Figure 12 shows a taper clamping coupling. Taper coupling creates the pressure with two wedged surfaces tightened against each other with screws.

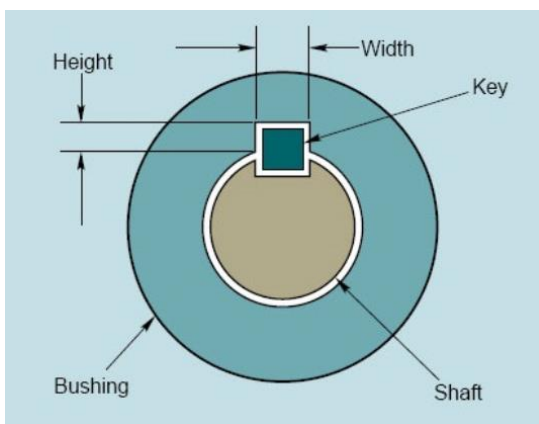


Figure 11. Keyed coupling (Santora, 2021)

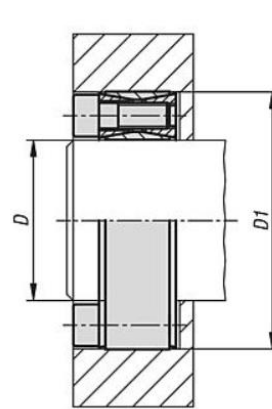


Figure 12. Taper clamping coupling (Norelem 2021)

Various types of rigid couplings can be found on the market. Manufacturers offer a lot of information from suitable couplings for specific applications. Design equations for

tolerances and e.g., hub stresses for each coupling type can be found from manufacturers datasheets. (Fenner drives 2012; Tollok 2003.)

Compliant couplings are basically modified rigid couplings. A coupling includes a rigid attachment into the shaft to be coupled and a deformable section between shafts. The deformable section is made from the material or geometry which can flex without high stresses or risk of fatigue. Several designs are made to offer different combinations of features. Table 2 reports common compliant couplings.

Table 2. Features of commercial flexible couplings. (Johnson Power LTD. 2021; Lovejoy-inc. 2021; Norton 2006, p.550-560; NTN Corporation 2005; RENK-group 2021; Regal Rexnord 2021; RW Couplings 2021)





Coupling type	Details	Misalignment tolerated		Picture
Jaw	Compliant member (between jaws) is made of rubber or soft-metal material. Attachment happens by friction in surfaces. Shock absorption capability. Backlash is unavoidable. Vibration damping capability.	Angular	$< 2^\circ$	
		Parallel	$< 3 \% \cdot d$	
		Axial	Slight	
		Torsional	Moderate	
Flexible-Disk	Deformation due to bending in plates and compliant member of elastomeric or metallic-spring material between plates and hubs. Slight shock absorption capability. Slight or no backlash. Slight vibration damping capability.	Angular	$< 3^\circ$	
		Parallel	$< 2 \% \cdot d$	
		Axial	Slight	
		Torsional	Slight or none	
Gear	Hub is in two parts where the inner part includes gear teeth and outer part internal teeth. Teeth can be straight or curved. No shock absorption capability. Slight backlash is unavoidable. No vibration damping capability.	Angular	$< 5^\circ$	
		Parallel	$< 0.5 \% \cdot d$	
		Axial	Large	
		Torsional	Slight or none	

Table 2. Continues

Coupling type	Details	Misalignment tolerated		Picture
Helical (beam)	One piece structure made of metal cylinder with helical slit. Slight shock absorption capability. No backlash. Slight vibration damping capability.	Angular	< 20°	
		Parallel	< 1 % · d	
		Axial	Slight	
		Torsional	None	
Bellows	One piece tube structure made from e.g., washer welded together. Slight shock absorption capability. No backlash. Slight vibration damping capability.	Angular	< 17°	
		Parallel	< 20 % · d	
		Axial	Slight	
		Torsional	None	
Rzeppa	Hub and shaft are grooved for small balls to transfer the torque (no bending resistance). No shock absorption capability. Slight or no backlash. No vibration damping capability.	Angular	Large	
		Parallel	None	
		Axial	None	
		Torsional	None	
Hooke	Hubs are attached with hinges which enables rotation with angular off set (no bending resistance). Rotational speed is not constant. No shock absorption capability. Slight or no backlash. No vibration damping capability.	Angular	Large	
		Parallel	None, Large in pairs	
		Axial	None	
		Torsional	None	
Elastomeric	Differs from jaw coupling in the way that jaws do not overlap, elastomer transfers the torque. Shock absorption capability. Backlash is unavoidable. Vibration damping capability.	Angular	Large	
		Parallel	Slight	
		Axial	Slight	
		Torsional	Moderate	

Table 2. Continues

Coupling type	Details	Misalignment tolerated	Picture
Grid	Two hubs are attached with a spring element which transfers the torque. Shock absorption capability. Slight or no backlash. Slight vibration damping capability.	Angular < 0.5°	

%·d means n percentage of the diameter

2.3 Machine dynamic design tools

When designing a machine, it is important to know the natural frequencies of parts and assemblies. Any system has infinite number of natural frequencies. (Norton 2006, p.102.) The frequencies which can be calculated is determined by the number of degrees of freedom of the system. Every frequency has a unique shape of vibration called a mode. (Logan & Chaudhry 2012, pp.782-786.) Natural frequency is determined mostly by system mass and stiffness. Damping has also an influence on natural frequency, but it mostly affects the amplitude of vibration. (Scheffer & Girdhar 2004, p.101.)

For vibration to happen, energy is needed in some form to excite it (sound wave, impulse, movement etc.). With rotating machines vibration excitation comes mainly from the machine itself. Those excitations can be due to e.g., unbalanced mass distribution or misalignment of two shafts. Both of those faults generate at least one vibration cycle per rotation. If rotating speed is the same as any natural frequency of the system, that will lead in very high vibration levels in the machine. The phenomenon is called resonance. (Mobius Institute 2021; Scheffer & Girdhar 2004, p.90, 94.) Thus, it is very critical to analyse possible resonances when designing a machine.

Narsakka (2020) has summarized in his study the excitation frequencies of vibration measurement of high-speed electric motor in post-assembly testing. Results show that rotational speed of the machine and its second, and third harmonic are avoided natural frequencies of machine when misalignment and unbalance may occur in the system.

(Narsakka 2020, p.32.) Sawalhi et al. (2019) have studied misalignment with a jaw coupling consisting of three jaws per flange. The study shows that at 3-times the rotating frequency there occurs excitation due to fluctuation of bending stiffness. (Sawalhi et al. 2019, p.132.) The structure of the coupling determines which harmonic occurs in the system but it cannot be accurately said which specific harmonic will appear in a certain case.

ISO 10437 (2004) sets a separation margin between a resonance frequency (critical speed, presented in the next chapter) and the operation speed. Separation margin is calculated from vibration response with help of amplification factor (F_a). Amplification factor can be calculated as:

$$F_a = \frac{n_c}{(n_u - n_l)} \quad (13)$$

Where n_c is frequency of critical speed, n_u and n_l are frequencies at both sides of the critical speed where vibration amplitude gets a value of $0.707 \times$ amplitude of top value of each critical speed (Figure 15). When the amplification factor is known the separation margin can be calculated as:

$$M_{s1} = 17 \left[1 - \frac{1}{F_a - 1.5} \right] \quad (14)$$

$$M_{s2} = 10 + 17 \left[1 - \frac{1}{F_a - 1.5} \right] \quad (15)$$

Where M_{s1} is the separation margin in case where the operation speed is higher than the critical speed and M_{s2} is valid for case where the rotating speed is lower than the critical speed. If the amplification factor is less than 2.5, resonance is considered critically damped and no extra margin is required. (ISO 10437 pp.22-23.) From the equation 15 can be seen that separation margin is 10% bigger when the critical speed is above operation speed.

2.3.1 Critical speed of the system

Study of the dynamic behaviour is usually started by analysing unsupported rotor natural frequencies and modes at the zero speed. Vibration response in this situation is called free-

free modes. Results can be used to evaluate the design on very first step. However, rotating part natural frequencies are changing over the speed due to gyroscopic effect which must be taken consideration when design decisions are made. In practise free-free results can be used for verification of analysis by comparing the analysis results to the experimental tests. On the other hand, when the design results are known to be correct, experimental results can be compared with the model to ensure e.g., proper attachment of disc or coupling. (Pyrhönen et al. 2009, p.46.)

When rotational speed is increased from zero, natural frequency separates into two frequencies. One frequency is decreased due to speed called as backward whirling mode (BW) and another one is increased called as forward whirling mode (FW). (Pyrhönen et al. 2009, p.46). When rotational speed intersects with BW or FW there is a high risk of resonance. Intersection of whirling mode is called as critical speed. (Dumitru et al. 2009, p. 394.)

Forced responses at critical speeds of the system can be calculated from equation of motion.

$$\mathbf{M}\ddot{\mathbf{q}}(t) + (\mathbf{D}_M + \Omega\mathbf{G}_M)\dot{\mathbf{q}}(t) + \mathbf{K}\mathbf{q}(t) = \mathbf{F}(t) \quad (16)$$

where \mathbf{M} , \mathbf{D}_M and \mathbf{K} are the matrices of system's moments of inertia, damping and stiffness properties. \mathbf{G}_M is a matrix of gyroscopic effects. $\mathbf{F}(t)$ is vector of forces generated from the system or applied external. $\mathbf{q}(t)$, $\dot{\mathbf{q}}(t)$ and $\ddot{\mathbf{q}}(t)$ are displacement, velocity, and acceleration of reviewed point in the system. When calculating only the critical speed, forces in the system can be set to zero. Then from the equation (16) damped eigenvalue problem is solved. (Dumitru et al. 2009, pp. 393-394.) Matrices can be formed with Finite Element Method (FEM) (Logan & Chaudhry 2012, pp. 4-10).

Campbell diagram is an important tool for easier evaluation of critical speeds at different speeds. It consists of a plot of natural and excitation frequencies at different speeds. (Dumitru et al. 2009, p. 393.) Guskov et al. (2007) have studied machine dynamics with a dual-shaft configuration test rig. They are presenting a Campbell diagram of the dual-shaft configuration where the second shaft has a constant speed relation (2.8) with shaft one.

Figure 13 shows the system BW (black line) and FW (bolded black line) modes, rotors speed and intersections of FW modes and rotors speed. (Guskov et al. 2007, p.5.)

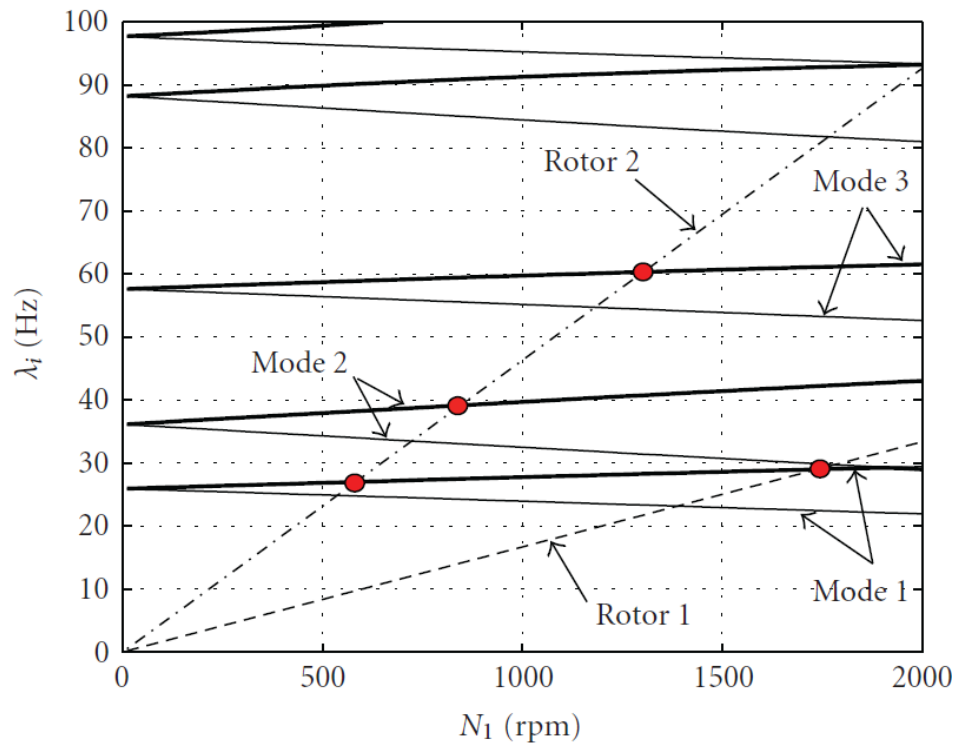


Figure 13. Campbell diagram of a dual-shaft rotor system presents critical speed of the system. Rotor 2 has constant 2.8 times the speed of rotor 1. (Guskov et al. 2007, p.5). Only FW modes have been marked with red dots when crossing critical speeds

As it can be seen in Figure 13 critical speeds are considered only with FW mode. From The measurement results of Guskov et al. can be seen that BW modes increase the vibration, but it has only a light deviation from steady state response. From the results one can see also that when the rotor goes over the first BW mode vibration direction moves temporarily against the spinning direction. When BW mode has been exceeded vibration returns in the same direction as spin speed, but it has a 90-degree shift compared with speed before BW mode. (Guskov et al. 2007, p.7.) Excitation which causes vibration with the same direction as spin speed like e.g., unbalance does not excite the resonance in BW mode, and it is usually left in less attention. Some fault like not properly preloaded ball bearings can cause asymmetric bearing properties which can lead the situation where unbalance also excite the BW mode (Pyrhönen et al. 2009, p.46). Three bearing AMB configuration is not well-known

technique, so it is important to also analyse and test the BW mode response with different scenarios.

2.3.2 Unbalance response

As it was discussed earlier the real system always contains some unbalance. In the design phase, it is good to analyse how unbalance at different locations affect the dynamic behaviour of the rotor. Unbalance mass (m_u) can be added to the simulation model and solved with equation 16. Unbalance forces (F_y, F_z) due to centrifugal force and unbalance mass can be written as:

$$\begin{bmatrix} F_y \\ F_z \end{bmatrix} = m_u r_u \Omega^2 \begin{bmatrix} \cos(\Omega t + \alpha) \\ \sin(\Omega t + \alpha) \end{bmatrix} \quad (17)$$

Where r_u is unbalance mass radius from the rotational axis, α is initial angular position of the unbalance mass and t is time. Lalanne and Ferraris (1998) presents widely known method step by step to solve displacements of rotor by using the equations 16 and 17. Choudhury et al. (2019) presents a case study of a paper roll where the same unbalance analysis is used in unbalance estimation. Figure 14 shows how the roll deflection changes when the unbalance location is changed in roll. The roll vibrates as 1st bending mode. The unbalance mass is located in blue line case into the left end (node 6) and in red line case into the right end (node 19). Thus, the support forces in the bearing generated from the vibrations changes between the cases. Similarly, in a 3 AMB system, the location of the unbalance affects the coupling support forces.

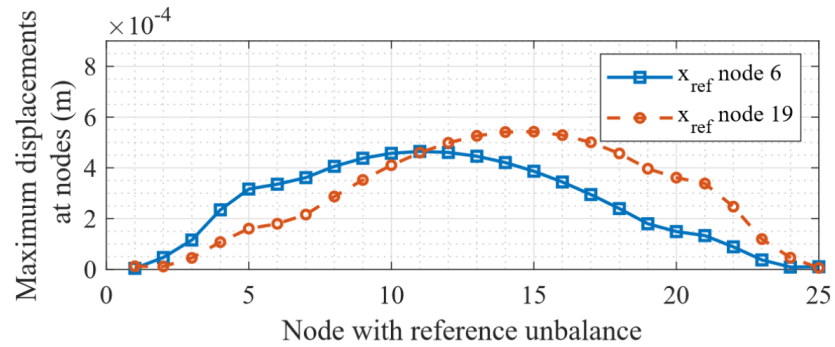


Figure 14. Deflection shape of tube roll with unbalance mass located at different nodes. (Choudhury et al. 2019, p.14)

Common way to evaluate the severity of responses caused by unbalance excitation is to plot the values in relation to rotational speed. From the figure one can see clearly how much critical speed affects the amplitude of vibration. Amplitudes in resonance were required for calculation of the separation margin of resonances (critical speeds) and operation range. Figure 15 shows a figure from ISO 10437 illustrating separation margin calculation. Unbalance in a selected node of rotor can be plotted at the same way and thus vibration response can be studied over the length of the drivetrain. Combining information from figures Figure 14 and Figure 15 shows how deflection in rotor changes in relation of speed, mode shape and unbalance.

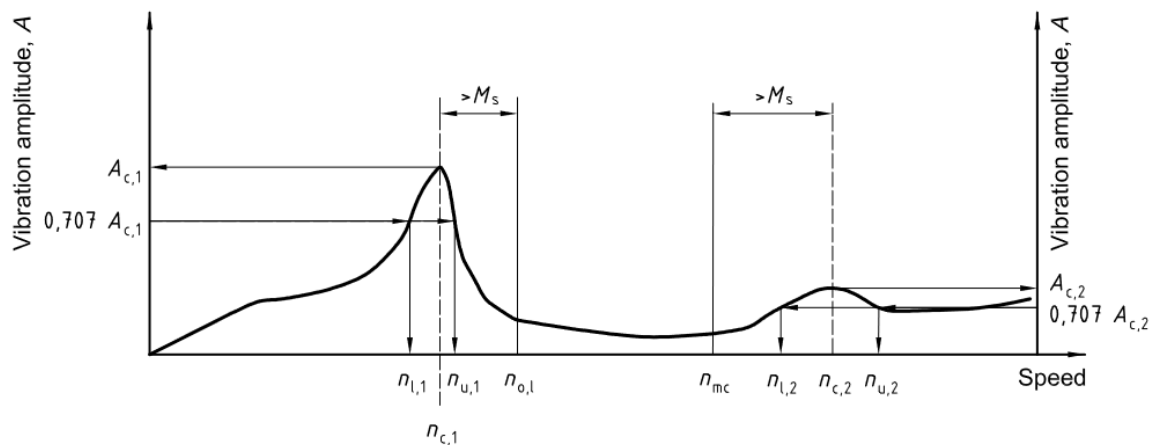


Figure 15. Vibration response over the speed to be utilized in separation margin calculation. (ISO 10437, p.23)

2.4 Methods for coupling's usability analysis

Up to this chapter the definition of baseline parameters set by drivetrain requirements have been described. In addition, it has been studied what kind of couplings are available on the market and how the machine dynamic analysis can be performed. The next step is to create a method for evaluating the couplings as part of a drivetrain. The focus of the work was in studying the mechanical characteristics of a coupling to make it possible to use various impellers with the same high-speed electric machine. The study hypothesis assumes that dynamic behaviour between electric machine and working machine can be minimized with the extension shaft supported by the third radial bearing. To confirm the hypothesis, one must define how the stiffness in a coupling affects the results. Stiffness values may not be offered from manufacturers in case of readymade components. So, those need to be analysed.

To make sure that possible solutions not just fulfil the stiffness properties, it must also be analysed how possible solutions can handle stresses from different usage situations.

2.4.1 Effect of coupling stiffness on drivetrain dynamic behaviour

The effect of the coupling stiffness can be analysed with motor shaft, extension shaft and different impellers. The extension shaft can be attached onto the rotor with an element whose stiffness values can be easily modified. For rapid calculation, beam model with a point stiffness is an effective method to utilize. Model can be made with special programs for rotor design. One such program based on beam element theory is RoBeDyn. It has been developed over a decade at LUT and it has been utilized in several studies (e.g., Kurvinen et al. 2021a,b; Choudhury et al. 2019; Pyrhönen et al. 2009). Results can be compared to solid element model with joint element between the shafts. FEA software ANSYS includes a bushing type joint which gives a possibility to compare the results between beam and solid element model. Figure 16 shows the mesh of a beam element model with the point stiffness between nodes 33 and 34. The impeller can be modelled as a point mass and bearing as a point supports.

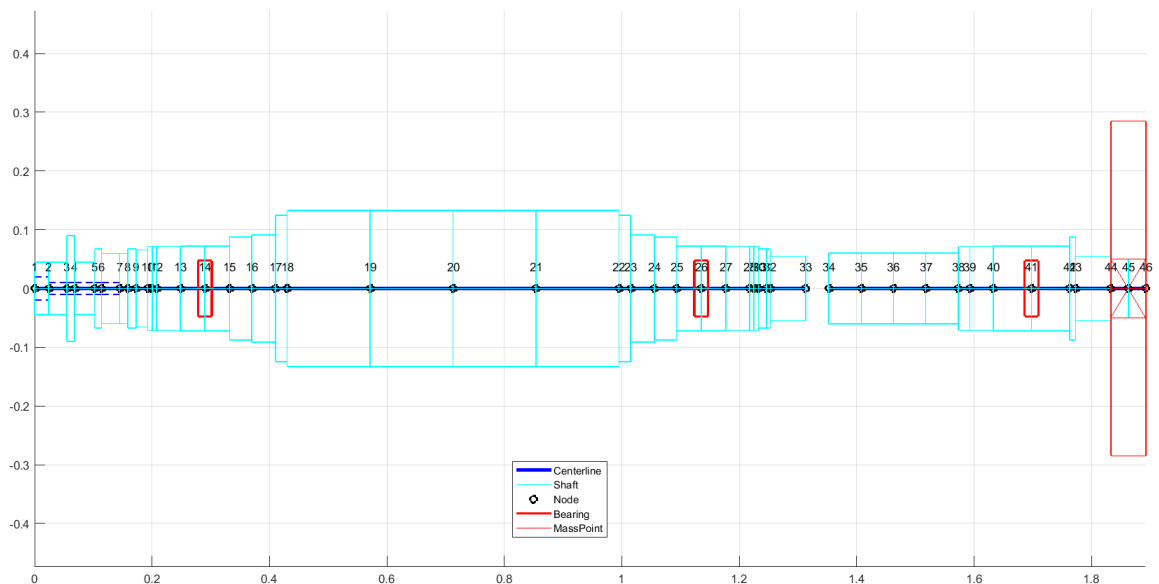


Figure 16. Drivetrain configuration in dynamical analysis divided into 46 nodes. Point stiffness can be inserted between the shafts i.e. between nodes 33 and 34.

By keeping the model the same but varying the stiffness values one by one it can be seen how the directional stiffness affects the natural frequency and mode shapes. That will give boundaries for more precise analysis.

2.4.2 Commercial coupling stiffness evaluation

The models designed in the design process must be analysed to know their stiffness properties. Commercial solutions may not include information of stiffness properties in the desired direction or rotation. One way to analyze stiffness properties is to utilise the same method as in previous chapter. Results of stiffness variation can be compared with model including the actual coupling. Another possible method is analysing the FE-model deformations in relation to forces or moments. That is easy and quick to do after the design sketch is ready which enables rapid design iterations. Translation can be analysed by inserting the force into the coupling surface in one direction. With spring rate equation (eq. 7) stiffness value can be solved from resulting directional displacement. Figure 17 and Figure 18 presents an example with a flexible disc coupling. In Figure 17 the coupling flange is fixed rigidly in any direction and force is set to the nearest surface of the flexible element. Directional deformation can be seen in Figure 18.

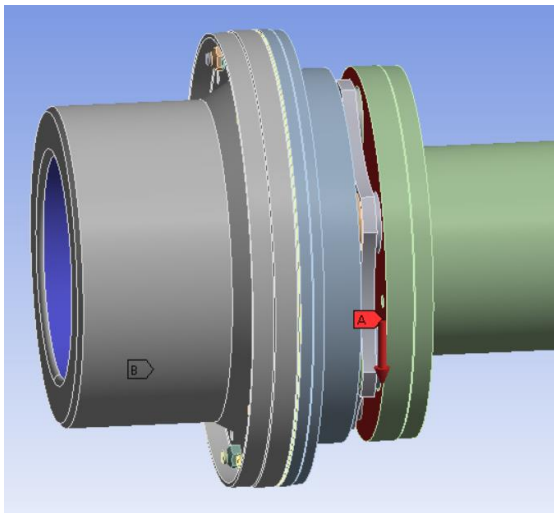


Figure 17. Disc coupling model for stiffness analysis. The blue surface is a supporting constraint and the red one is the inserted force.

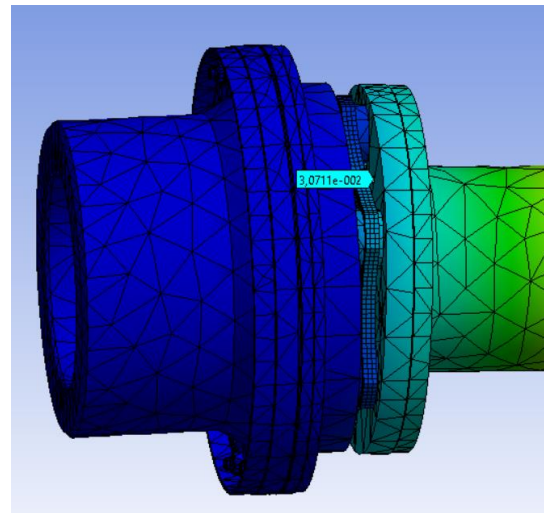


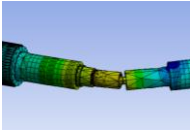
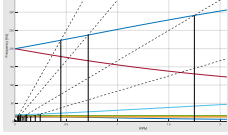
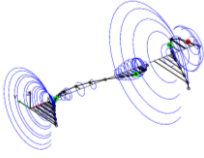
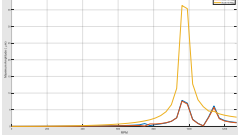
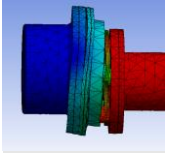
Figure 18. Directional displacement value can be analysed with FE-method.

With the same method the stiffness values in any direction and rotation can be calculated. With rotation in the equation, force is replaced with torque and displacement must be converted into rotation, results are then Nm/rad.

2.4.3 Coupling behaviour estimation in usage

For those coupling models which fulfil the requirement of power transfer and stiffness properties, can be used in drivetrain analysis. Analysis can be made with the same RoBeDyn model as stiffness variation has been made by adding the coupling details in the model. Critical speeds and mode shapes are analysed to see how deflection appears in the system. With unbalance response analysis relative displacement over the coupling can be estimated. Relative displacement can be used to analyse the stresses in the coupling with solid element model via e.g., ANSYS software. Table 3 presents the steps of evaluation.

Table 3. Steps for operational evaluation of different coupling types.

Drivetrain model	Critical speeds	Operational mode shape	Unbalance response	Stress analysis
				

Shafts with simple cross sections can be analysed with analytical equations to calculate stresses in coupling. When displacement between two points is known equation (11) can be modified to calculate stresses in a coupling. When the cross section and moment in the coupling are known the stress can be calculated with

$$\sigma_b = \frac{Mc}{I} \quad (18)$$

Where σ_b is stress from the bending, M is the moment which can be expressed FL , and c is the distance from cross section's neutral axis to the farthest surface on the cross section. (Budynas, & Nisbett 2015, p126) Combining equations 11 and 18 gives the stress as:

$$\sigma_b = \frac{\delta 3Ec}{L^2} \quad (19)$$

3 RESULTS AND ANALYSIS

This chapter presents how the coupling design for the case study has been implemented using the methods from chapter 2. The first sub-chapter is defining the initial requirements for the design. The following subchapter presents the baseline calculations and analysis of potential couplings in same order than presented in chapter 2.

3.1 Requirements for the system

As there is no direct standard for the system, ISO 10441 defined for the corresponding four-bearing system is used as reference. The main initial requirements for the coupling were torque and speed. The maximum speed for the motor was informed to be 16000 rpm (Kurvinen et al. 2021a p.5). The steady state torque was presented to be 1670 Nm.

The coupling must be designed to be able to transmit 115% transient torque of induction motor (ISO 10441 p.11). During the full voltage starting the transient torque can be in as high as 200 – 300 % of the pull-out torque (Wahl & Kilgore 1940, p.603). And the pull-out torque is in range 200 – 300 % of steady state torque (Musgrove et al. 2019). Then the case study maximum design torque reach at level 12003 Nm ($1670 \text{ Nm} \cdot 1.15 \cdot 2.5 \cdot 2.5 = 12003 \text{ Nm}$).

The fatigue load safety factor is set to be minimum 1.25 when using a Goodman diagram. With the load being the maximum angular misalignment and the maximum axial displacement of coupling. (ISO 10441 p.12.) The maximum residual unbalance grade is 2.5 mm/s according to ISO 21940-11 with the case study drivetrain in commissioning state. In the worst case, the unbalance is estimated from breakdown of turbine blade. One turbine blade mass is analysed from 3D model and its mass is 6.3 g at impeller radius of 276 mm. Equation 9 calculates for the unbalance class G 71 when one blade comes off from the outer perimeter.

3.2 Baseline values for the coupling

Initial requirements for the drivetrain presented in the previous chapter are used as inputs for the baseline calculation presented in chapter 2.1. The maximum and the minimum diameter for the cross section of the coupling regarding the speed and the torque of the system are presented in the first sub-chapter. The second sub-chapter presents the required radial stiffness with different extension shaft configurations. The last sub-chapter presents the result as a baseline model.

3.2.1 Maximum and minimum values for coupling cross section

Calculations were started by calculation of minimum circular cross section with equation 5 based on transient torque during a start-up (12003 Nm). Next the needed diameter against fatigue loading was evaluated with equation 4. Only torque load was considered at this point. Steady state load (1670 Nm) was used for mean torque and 20 % fluctuation from steady state as an amplitude. Stress concentration factor for torsion was 2 in calculations. The exact value cannot be determined at this point because the factor depends on the attachment type (Pilkey 1997). After torque requirement the maximum diameter for solid and hollow cross sections were calculated regarding the angular velocity of system based on equations (2) and (3). Table 4 presents the results of the calculations with structural steel grades 355 and 700.

Table 4. Minimum and maximum diameters calculated from torque and velocity requirements for coupling. Values are in mm.

Cross section	Loading	Yield stress 355 MPa	Yield stress 700 MPa
Solid	Static torque, min. D	58.5	46.5
	Fatigue torque, min. D	52.5	42
	Velocity, max. D	229	321
Hollow *	Velocity, max. d	180	260
	Velocity, max. D	213	298

* Wall thickness affects the results according to equations (2) & (3). Target wall thickness was set $\sim 0.1 \times$ outer radius.

As can be seen in Table 4 the fatigue diameter was obtained to be less than in the static case, which can be explained by the high transient torque. Thus, by dimensioning according to the

static case, the fatigue load consideration becomes fulfilled at the same time. With 33 % fluctuating torque load, diameter based on fatigue design gets the same diameters than with static load design. It should be noted that the transient torque is large compared to the steady state torque. Because the transient torque lasts only a short period of time some of the load goes for the moment of inertia of the rotor, and thus, full torque is not to be transmitted to the coupling. If transient torque is lowered to half from the original, the minimum diameters get values of 46.5 mm / 37 mm (S355 / S700) and with those diameters fluctuating torque can be 9% from steady state torque. The minimum wall thickness is not reported for the hollow cross section, because the wall thickness goes less than one millimeter with an outer diameter with an outer diameter greater than 128 millimetres if only yielding is considered. With thin structures the failure criteria of the cross-section can no longer be assumed only based on the yielding (Timoshenko 1983).

3.2.2 Demanded radial stiffness from static equilibrium

Next the static equilibrium of the system was calculated according to chapter 2.1.3. The calculation results show the preliminary stiffness needed from the coupling to be able to handle the gravity and unbalance forces in the system. Required stiffness is calculated in 4 cases. Cases are illustrated in Figure 19.

1. G 2.5 unbalance with case study configuration.
2. G 71 unbalance with case study configuration.
3. G 2.5 unbalance with 60 kg impeller, + 50 mm cap between impeller and safety bearing, short (50 mm) extension shaft configuration.
4. G 71 unbalance with case 3.

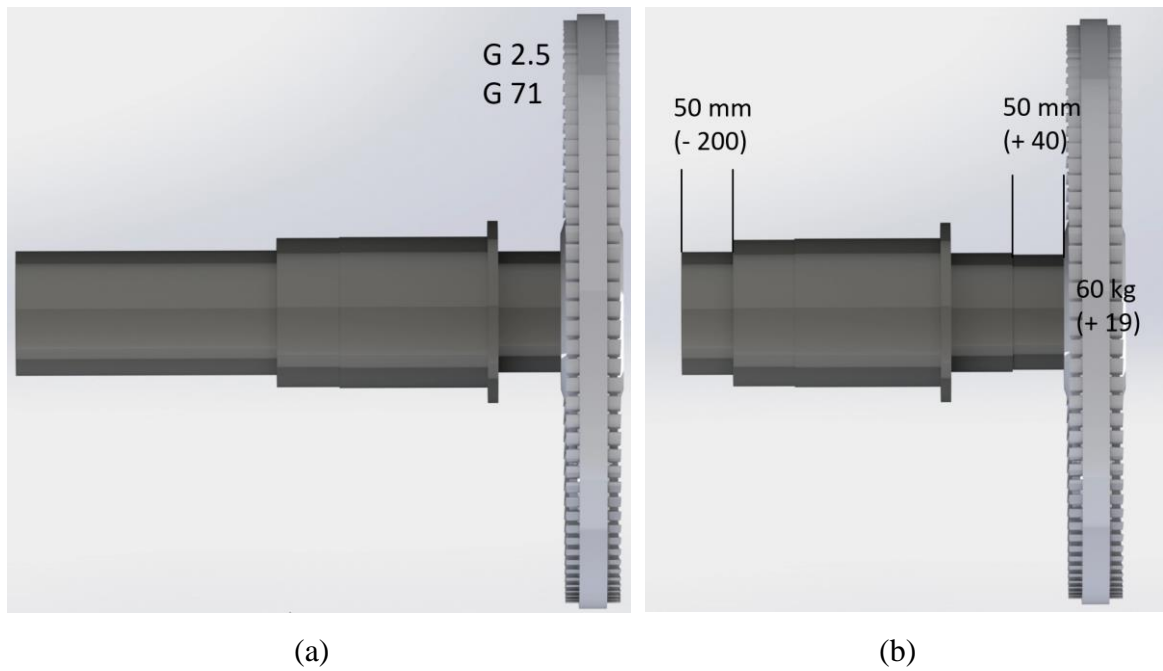


Figure 19. Case study extension shaft configuration with unbalance grades 2.5 and 71. (b) Extension shaft configuration with possible design changes.

Case 3 and 4 present the situation when changing the extension shaft configuration coupling support force increases the most according to equation (10) (in equation (10) the length of the x3 decreases (-200 mm) and x2 increases (+40 mm)). Table 5 shows the required radial stiffness calculated from equation (7) and (10) with 20 μm acceptable displacement. Which can be calculated from equation (6) using 270 μm for minimum cap clearance and 4 by dynamic factor.

Table 5. Radial stiffness required from the coupling with four different cases.

Case	Required radial stiffness (N/m)
1	$13.9 \cdot 10^6$
2	$79.1 \cdot 10^6$
3	$63.3 \cdot 10^6$
4	$232.8 \cdot 10^6$

3.2.3 Baseline values as a baseline model

After the cross-section definition and lateral support stiffness evaluation, length of the baseline model can be determined with equation 12. In Table 6 and Table 7 are presented the results with previously calculated diameters and minimum stiffness values.

Table 6. Length for coupling baseline model with solid circular cross section. Dimensions are in mm.

Radial Stiffness (N/m)	Diameter S355	Length	Diameter S700	Length	Diameter S700*	Length
$13.9 \cdot 10^6$	58.5	296.5	46.5	218.3	42	190.6
$79.1 \cdot 10^6$	58.5	166.1	46.5	122.3	42	106.8
$63.3 \cdot 10^6$	58.5	178.9	46.5	131.7	42	115.0
$232.8 \cdot 10^6$	58.5	115.9	46.5	85.3	42	74.5

*Required diameter based on fatigue calculation.

Table 7. Length for coupling baseline model with hollow circular cross section.

Radial Stiffness (N/m)	D in	D out	Length	D in	D out	Length
$13.9 \cdot 10^6$	180	213	1309	260	298	1946
$79.1 \cdot 10^6$	180	213	733	260	298	1090
$63.3 \cdot 10^6$	180	213	789	260	298	1174
$232.8 \cdot 10^6$	180	213	511	260	298	760

S355 steel grade requires a larger diameter than S700 for torque capacity. However, strength does not affect the deflection and deviation of elastic modulus between steel grades are low. Thus, the ratio between the length and diameter of baseline coupling does vary a much depending on the steel grade. Figure 20 illustrate the ratio between the length and diameter with Table 6 cases. As can be seen in the Figure 20 with the highest demanded radial stiffness (case 4) the maximum length of the baseline coupling is required diameter multiplied by 2.

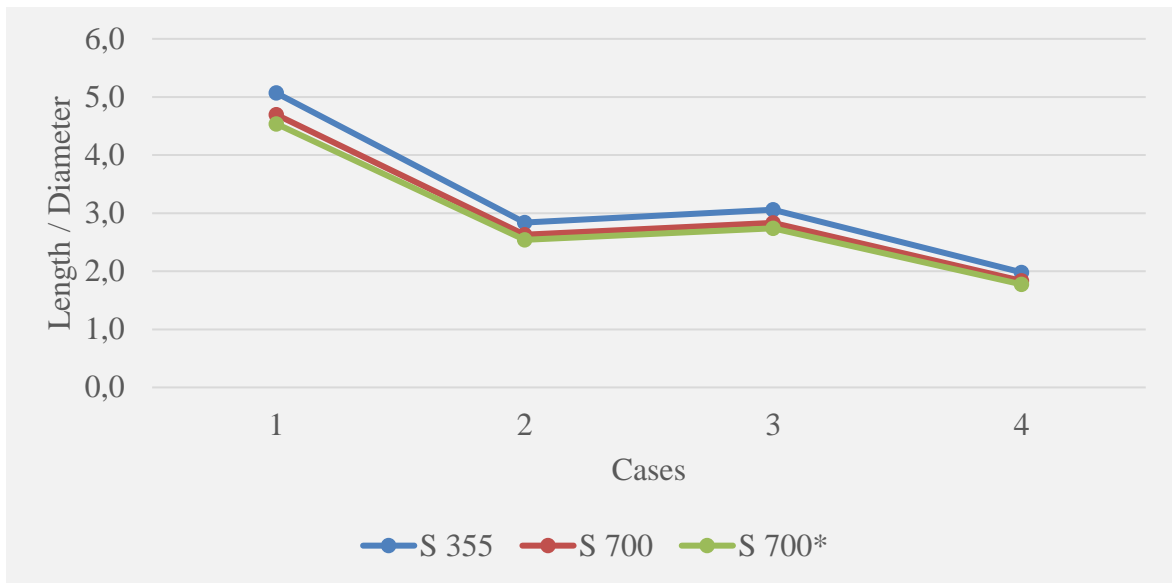


Figure 20. Ratio between the length and diameter of baseline solid cross section with different radial stiffness required from the coupling, calculated with Table 5 and Table 6 values.

3.3 Evaluation of commercial couplings

Existing couplings suitable for high-speed applications are made to operate between two separate machines (Figure 3, b). The couplings between two machines are required to be flexible avoiding the forces due to angular or parallel misalignment. To ensure misalignment capacity some couplings are designed with two flexible elements. In the case study extension shaft is supported only by one bearing, and thus, coupling can include only one flexible element in the coupling (with two flexible element or joint the system becomes a mechanism). The following table summarizes the operating values informed by the coupling manufacturers. Required radial stiffness is selected based on case 2 from previous chapters. Values are painted in table where colours mean, red incompatibility, green compatibility and yellow near the limiting value.

Table 8. Coupling parameters to match initial requirements. (Lovejoy-inc. 2021; RW Couplings 2021; RENK-group 2021; Johnson Power LTD. 2021; Regal Rexnord 2021; NTN Corporation 2005;)









Coupling		Rated speed (rpm)	Rated torque (Nm)	Lateral stiffness (N/m)
Required		16 000	1 670	79
	R+W EK6 2500	10 000	2 450	Low
	R+W SP6 450	18 000	660	Low
	R+W BK2 1500	20 000	1 500	3.6
	R+W BK2 10000	4 000	10 000	21.8
	RENK Raflex DTM 133	19 000	3 950	330*
	Regal Rexnord RMS 4704	20 700	20 789	High
	RENK ZTK 63	25 000	4 900	High
	R+W BZ1 25	4 550	2 900	High
	NTN global BJ225	1 200	2 940	High
	Johnson Power LTD. 81	4 500	1 560	High
	Regal Rexnord Elastomeric™ 100	1 800	8 813**	Low

Table 8. Continues.

Coupling		Rated speed (rpm)	Rated torque (Nm)	Lateral stiffness (N/m)
Required		16 000	1 670	79
	Lovejoy-inc Grid 1090	3 600	3 728	Moderate
	Regal Rexnord KOP-GRID	4 000	3 389	Moderate

*Analyzed from 3D model by FEM **Peak torque

With helical type coupling it was not possible to find any solution to match even close to the torque or speed requirements. As can be seen in Table 8 most of the couplings fulfil only speed or torque requirements. Lateral stiffness values could only be found for the bellows type coupling. RENK Raflex DTM 133 3D model was obtained from manufacturer and its lateral stiffness was analysed with the method presented in chapter 2.4.2.

3.4 Usability of couplings in three AMB drivetrain configuration

Up to this phase of results commercial couplings suitability and baseline model are evaluated based on the coupling parameters as a single unit. However, as noted before high-speed drives cannot be designed as individual components. Coupling does not connect only speed and torque between machines but also dynamics of the machines. According to the previous studies, the stiffness of the coupling affects the performance of the drivetrain, thus first is presented how coupling stiffness affects the natural frequency of the drivetrain. In second sub-chapter is analysed commercial disk coupling stiffness parameters for beam element analysis. In third and fourth sub-chapter is analysed full drivetrains with baseline and disc couplings.

3.4.1 The effect of coupling stiffness on drivetrain dynamics

Calculations for coupling stiffness evaluation was performed with the method presented in chapter 2.4.1. Figure 16 in chapter 2.4.1 shows the configuration which has been used in

calculations. Radial, bending, axial and torsional stiffness values were varied between $1 \cdot 10^3$ to $1 \cdot 10^{12}$ (N/m and respectively Nm/rad). One direction has been analyzed at once and other values is kept in $1 \cdot 10^3$ value through the analysis. Figure 21 presents the natural frequency of the drivetrain with varying stiffness values. Solid lines with dots present the variation of radial stiffness and dashed lines variation of bending stiffness.

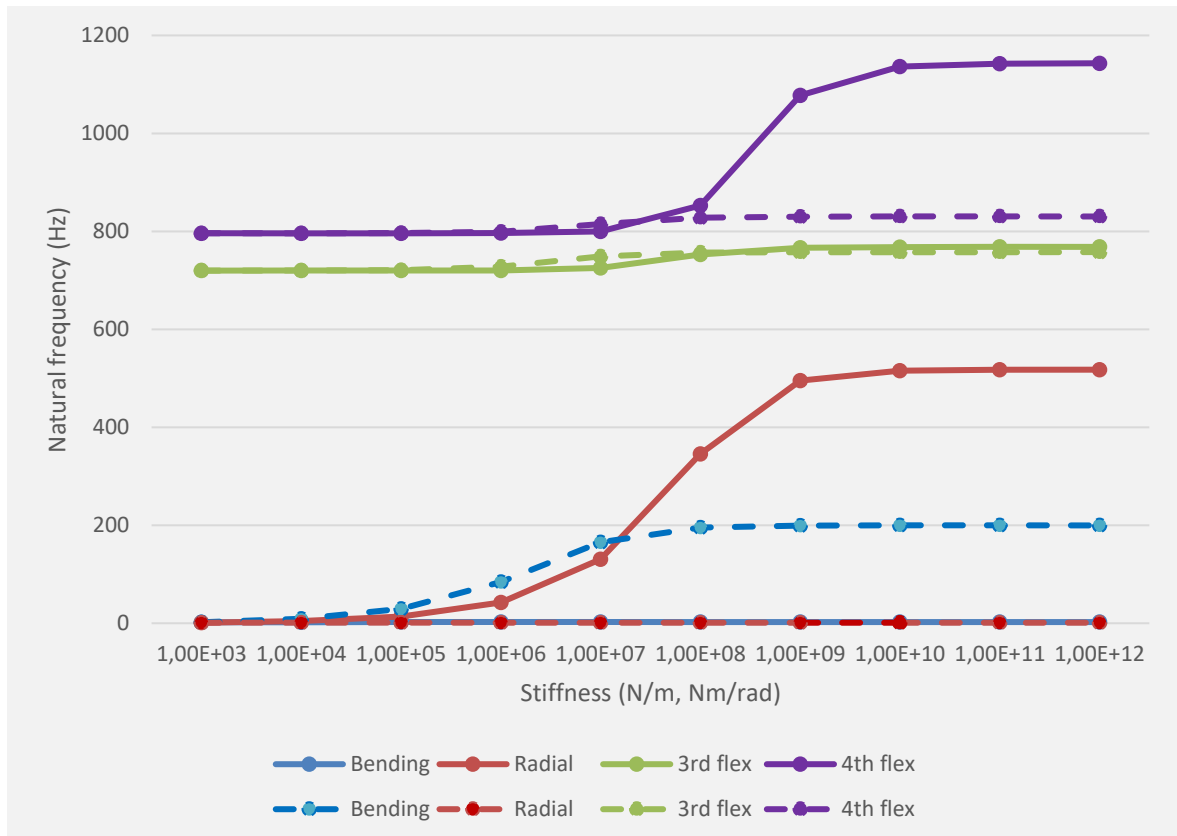


Figure 21. Effect of coupling stiffness to the natural frequency (free-free) of the case study drivetrain. Solid lines present the variation of radial stiffness and dashed lines variation of bending stiffness.

As can be seen in Figure 21, the 3rd and 4th frequencies are above 700 Hz (42 000 rpm) with any stiffness value. So, those modes do not interfere with the operation range with any specified stiffness values. The 1st flexible mode frequencies do not change practically at all in relation of one direction evaluated at the time. That is due to reason that the 1st flexible mode shape changes between radial (Table 9, row 2) and bending (Table 9, row 1) due to stiffness variation. So, practically when keeping other value $1 \cdot 10^3$ N/m (Nm/rad) its frequency stays in that level regardless the stiffness in other direction. The radial mode

(rocking mode in Table 9, row 2) frequencies have the biggest change in frequencies and those pass through the operation range of drivetrain.

In real coupling it may not probably be possible to make only one direction with high stiffness. Figure 22 presents results when radial and bending stiffnesses are varied at the same time with the same value. Axial and torsional stiffnesses are kept at their original values. Black lines with black dots show the simultaneous variation when other lines are presented as previous.

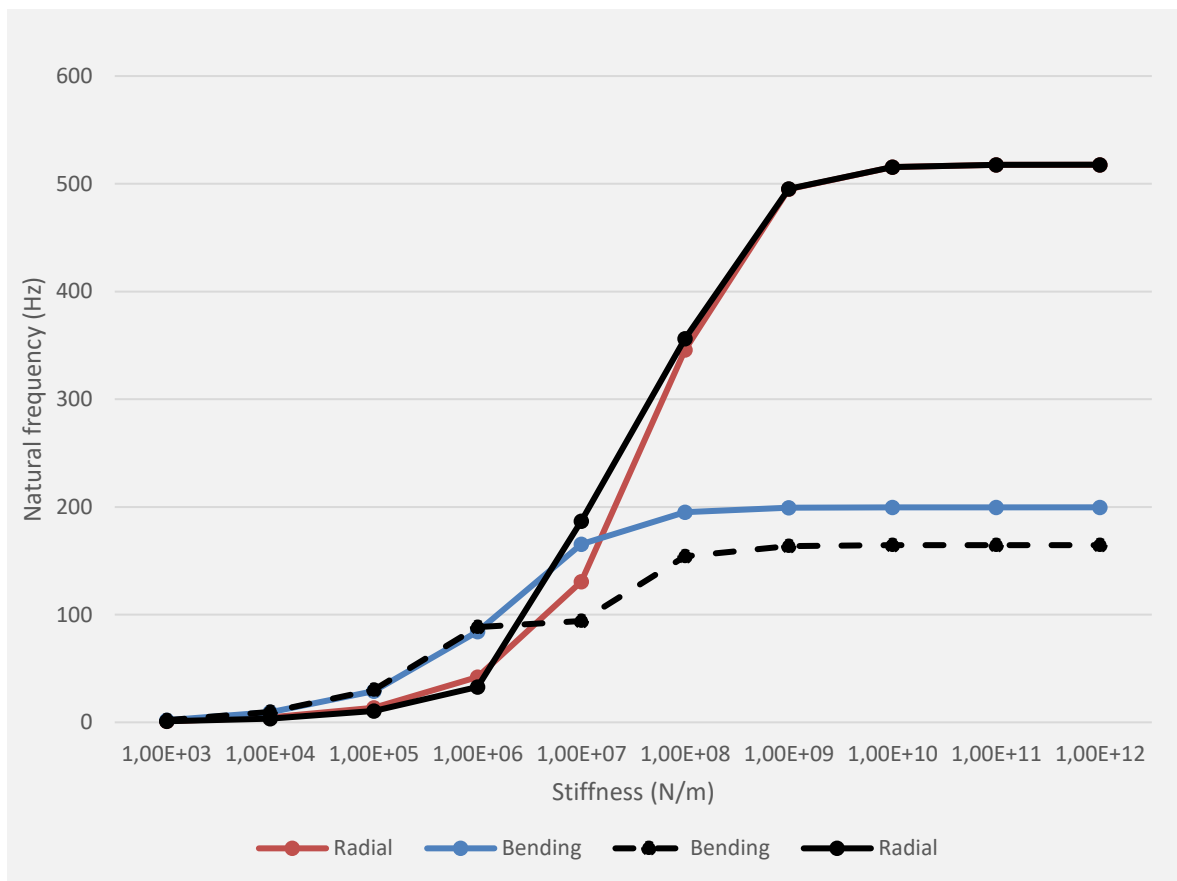


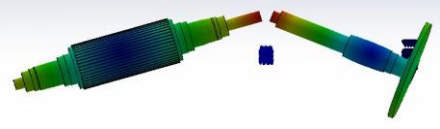
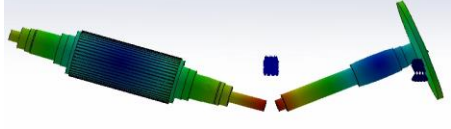
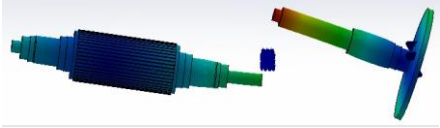
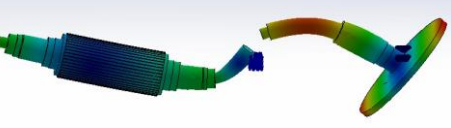
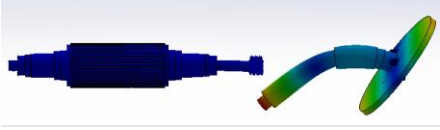
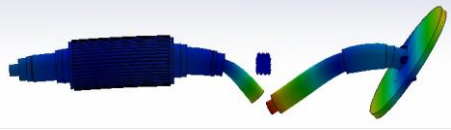
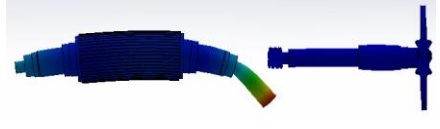
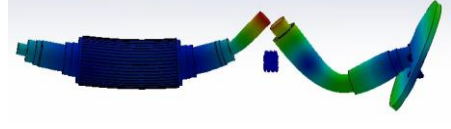
Figure 22. Effect of coupling stiffness to the natural frequency of the case study drivetrain. Solid lines with black dots present the simultaneous variation of radial and bending stiffness when other lines are as in Figure 21.

The radial mode follows near the individually varied radial natural frequency values. Only in $1 \cdot 10^7$ N/m value combination results differ by over 5 % (11,5 %) from individual variation. The effect of simultaneous varied stiffnesses occurs in more surprising way in the bending mode natural frequencies. It follows near the individually varied bending mode but

has a lower natural frequency. The biggest deviation in results occurs when radial and bending modes frequencies come close to each other. It looks that it causes the radial frequency to occur at a higher and bending frequency at lower level.

Solid element model was created with SolidWorks software to analyse axial and torsional frequencies and to confirm previous presented RoBeDyn results. Solid element model presents the mode shapes also easily understandable 3D figures. Table 9 shows the case study drivetrain mode shapes with $1 \cdot 10^6$ and $1 \cdot 10^8$ N/m stiffness values (the same value in all directions). Rotor and extension shaft ends has been modified to highlight the shape of mode.

Table 9. Mode shapes of case study drive train with $1 \cdot 10^6$ and $1 \cdot 10^8$ point stiffness values.

Mode number	Mode shape, $1 \cdot 10^6$ N/m (Nm/rad)	Mode shape, $1 \cdot 10^8$ N/m (Nm/rad)
1 st		
2 nd		
3 rd		
4 th		

From the Table 9 can be seen that the mode shapes change totally between $1 \cdot 10^6$ and $1 \cdot 10^8$ N/m values. Modes 3 and 4 show difference very clearly. With value $1 \cdot 10^6$ N/m, 3rd mode corresponds directly to the extension shaft's individual 1st flexible mode (as it been analysed separately). The same thing is visible from in the 4th mode with rotor individual 1st flexible. When shafts are coupled with $1 \cdot 10^8$ N/m stiffness value the mode shape bends uniformly. The same phenomenon can be seen also from 2nd mode. From the 1st mode one cannot be

seen difference in shapes, in both cases bending appears in coupling and shafts are vibrating almost as rigid shafts.

Torsional natural frequency varies under 100 Hz, and it will be below the operation range with any torsional stiffness value. Axial results differentiate significantly as can be seen in Figure 23 and it may conflict with operation range.

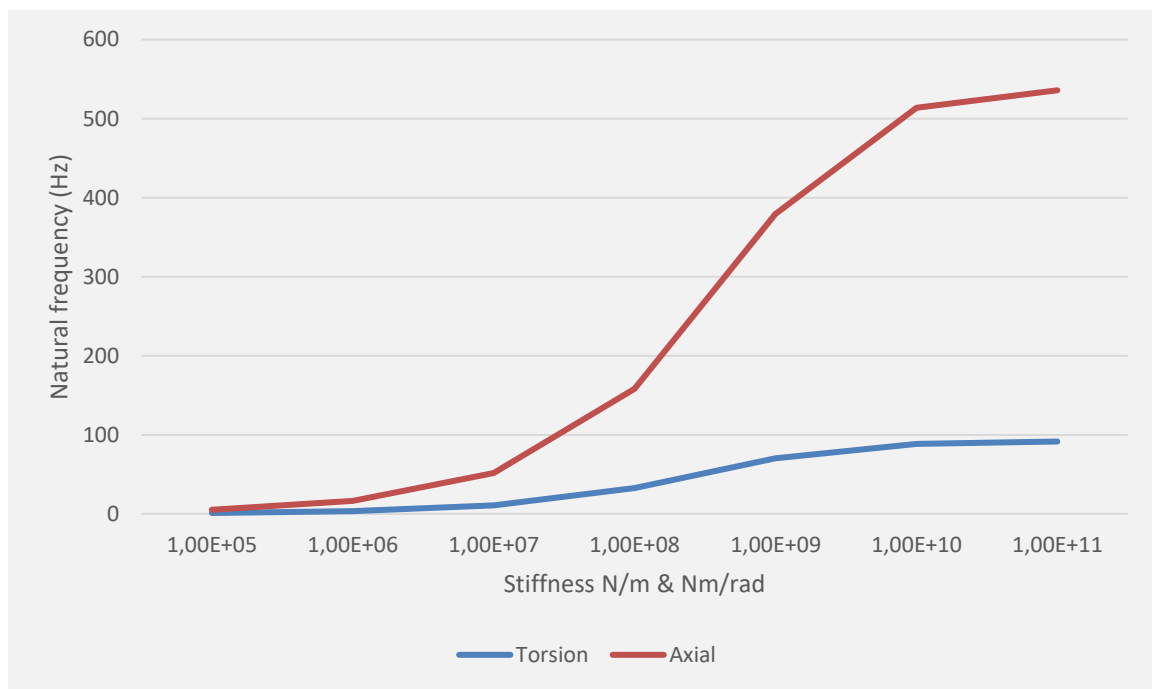


Figure 23. Effect of torsional and axial coupling stiffness on the natural frequency of the case study drivetrain.

3.4.2 Disc coupling stiffness analysis

Based on the ability of commercial couplings to satisfy torque and speed requirements, a disc coupling was selected for further analysis. The RENK Raflex DTM 133 coupling model with torsion sensor capability match the purpose of case study configuration. From that coupling only one side of coupling is used (one flexible element) in the three-AMB configuration. Figure 24 present the 3D model of the coupling. The right side flange is used normally with installation of torsion sensor but in case study it could be used for extension shaft attachment.

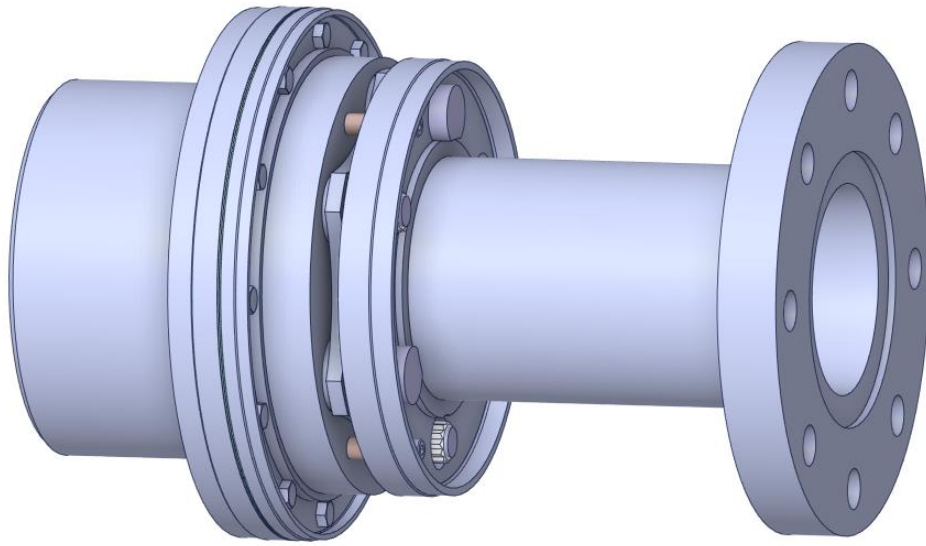


Figure 24. Half of the RENK Raflex DTM 133 coupling model with torsion sensor capability.

For beam element analysis plate section stiffness properties are needed. They were analyzed with Ansys 2021 R1 software. 5 load steps were used in the analysis for possible change in stiffness caused by loading. Appendix I presents the results for all analyses. However, any significant variation was not found from analysis. Table 10 shows directional stiffness values obtained from analysis.

Table 10. Disc coupling directional stiffness values.

Direction	Stiffness	Unit
Torsional	$2.80 \cdot 10^6$	Nm/rad
Bending	$1.21 \cdot 10^5$	Nm/rad
Axial	$3.87 \cdot 10^7$	N/m
Radial	$3.17 \cdot 10^8$	N/m

3.4.3 Usability of baseline coupling model in drivetrain

For drivetrain design it would be beneficial to create easily modified coupling. Solid circular cross section (called later as thin shaft) fulfils excellently that demand. Drivetrain was

modelled with rigid attachment between coupling and shafts. Figure 25 shows the drivetrain configuration with baseline model coupling.

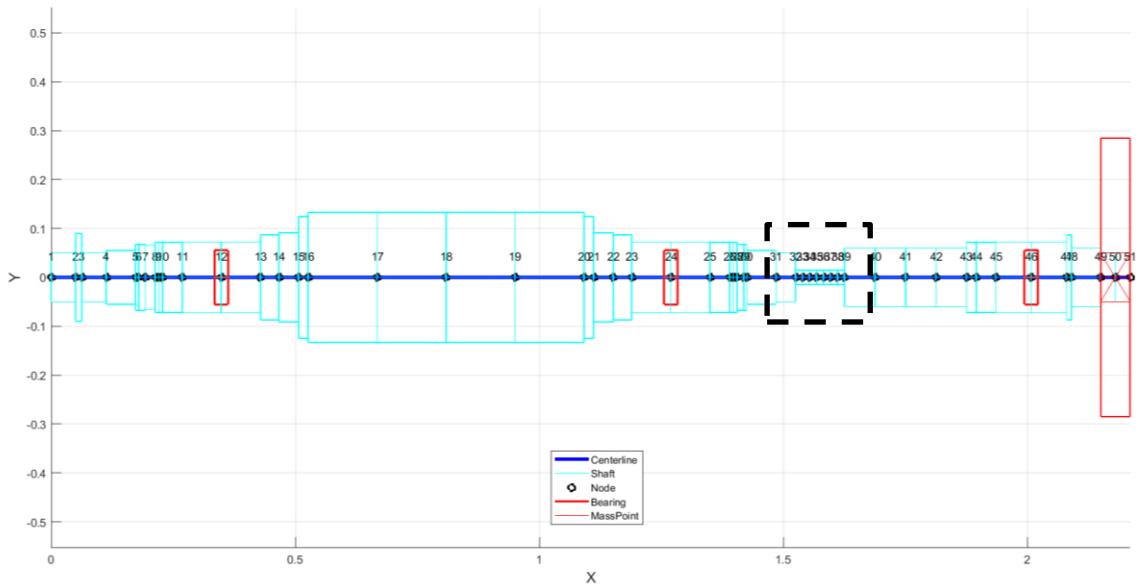


Figure 25. Case study drivetrain configuration with baseline model coupling.

Minimum diameter of the thin shaft based on transient torque was calculated to be 46.5 mm. However, analysis for baseline model was started with $D = 30\text{mm}$ and $L = 100\text{mm}$ geometry (Figure 25) to create understanding of dynamic behaviour in wider range. Table 11 presents the natural frequencies in zero speed with different thin shaft configurations. The last three lines are case study baseline model for G71 residual unbalance.

Table 11. Natural frequencies of drivetrain with different thin shaft dimensions.

$D \times L$ (mm)	1 st flexible freq. (Hz)	2 nd flexible freq. (Hz)	3 rd flexible freq. (Hz)	Gap from 1 st to 2 nd flexible freq.
30 x 100	19	297	597	278
40 x 100	33	351	613	319
50 x 100	49	372	621	324
60 x 100	65	382	626	318
30 x 50	27	382	626	355
40 x 50	45	397	633	352
50 x 50	65	404	637	339
60 x 50	82	409	641	327
58.5 x 166*	50	339	607	290

46.5 x 122**	39	348	612	309
42 x 106***	35	351	613	316

*With S355 **With S 700 ***Required diameter based on fatigue calculation with S 700.

The thin shaft parameters do not appear to affect the frequencies of the 3rd flexible shape significantly (maximum deviation 6.9 %). In the 2nd mode deviation between the smallest and the largest frequency is 27.4 %. When, 1st mode deviation reaches to 76.8 %. The widest gap between the 1st and the 2nd modes can be achieved with the 30 × 50 mm thin shaft model. With the 40 × 50 mm model the gap is in the same level, but 1st flexible mode is considerably lower level. From baseline models the thinnest diameter generates the largest gap between modes, creating lowest 1st and highest 2nd mode.

Mode shape plot reveals the shape of shaft's vibration. Figure 26 presents the mode shapes of case study drivetrain with 46.5 × 122 mm baseline thin shaft coupling. The 2nd mode crosses the centre line (nodal location) in rotor's right AMB sensor location (node 26) which is not a desirable situation. Also, the 1st mode second nodal location is near the third AMB sensor position (node 42). The dominant shape change due to speed and thus more specific shapes can be analysed with whirling mode shapes.

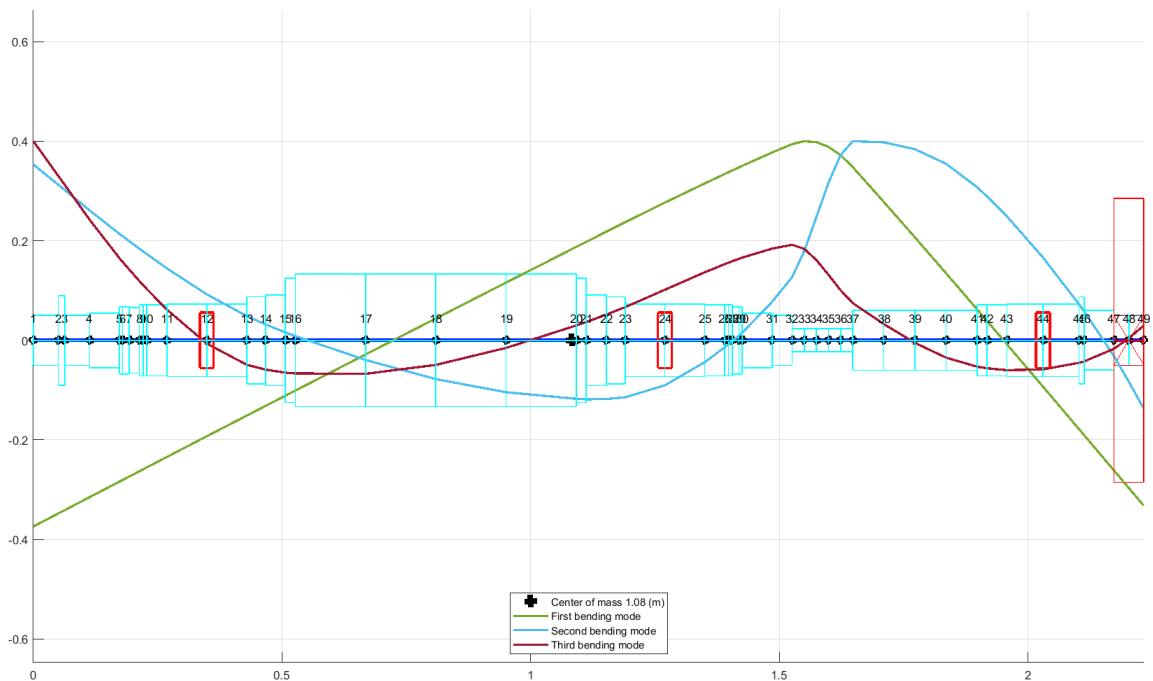


Figure 26. Mode shapes of the case study drivetrain with $D = 46.5$ mm and $L = 122$ mm thin shaft coupling.

With 46.5×50 mm thin shaft configuration the 2nd mode nodal locations does not appear at sensor positions as can be seen from Figure 27. With the 1st mode does not happen significant changes in nodal locations.

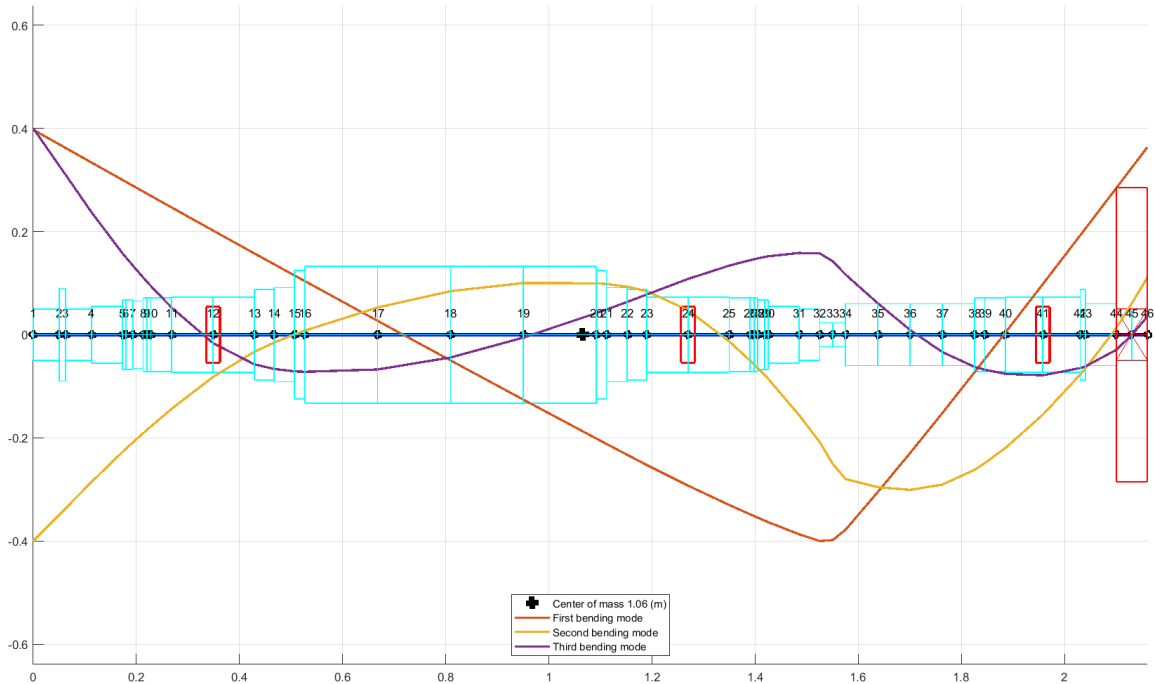


Figure 27. Mode shapes of case study drivetrain with $D = 46.5$ mm and $L = 50$ mm thin shaft coupling.

Frequencies presented in Table 11 changes with rotational velocity. With Campbell diagram can be easily see how the response change over the speed. In Figure 28 and Figure 29 is presented Campbell diagram for baseline couplings (46.5×122 mm and 46.5×50 mm) with 1-, 2- and 3-times rotational frequency (dashed lines). Vertical black lines indicates when 1-, 2- or 3-times rotational frequency (1X, 2X, 3X) cross the natural frequency of drivetrain indicating the critical speeds, only forward modes are assumed to be critical ones. The blue dashed line box depicts the operating range of the machine with 20% safety margins. Neither configuration has not a 1X critical speed in the operating range. 2X and 3X occur in the operating range. With a 46.5×122 thin shaft, the 2X critical speed is close to the rated speed, it could be a problem if misalignment occurs in the drivetrain.

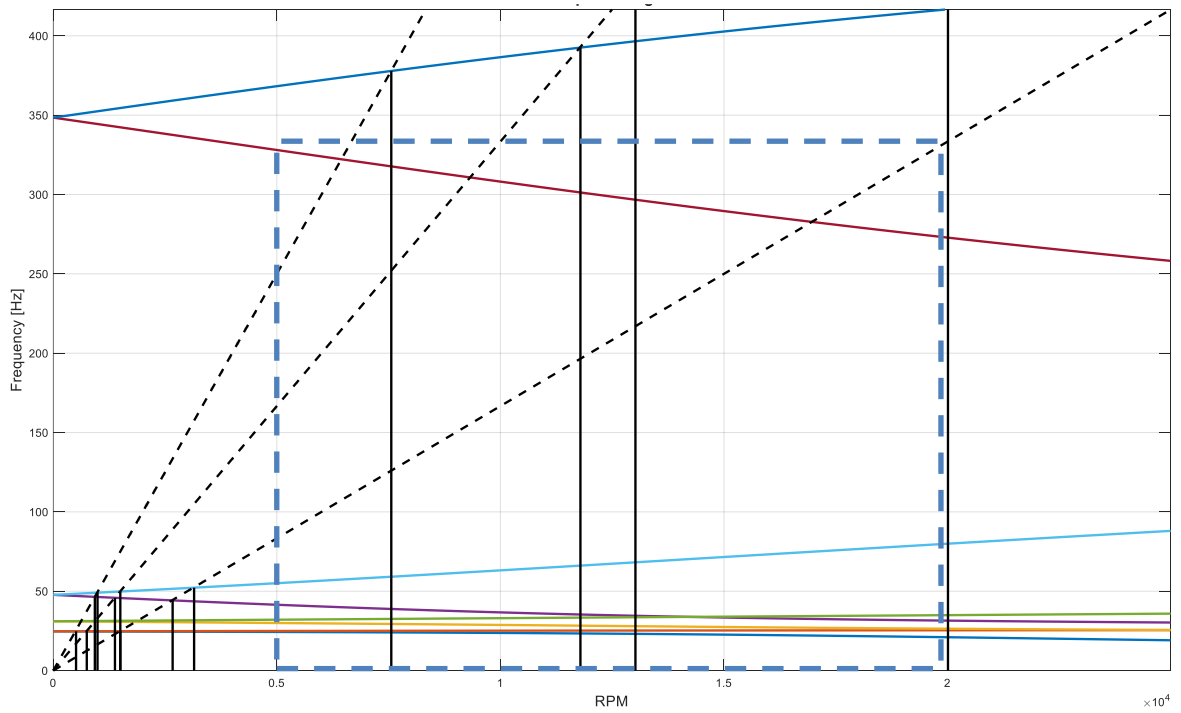


Figure 28. Campbell diagram of case study drivetrain with 46.5×122 mm thin shaft coupling.

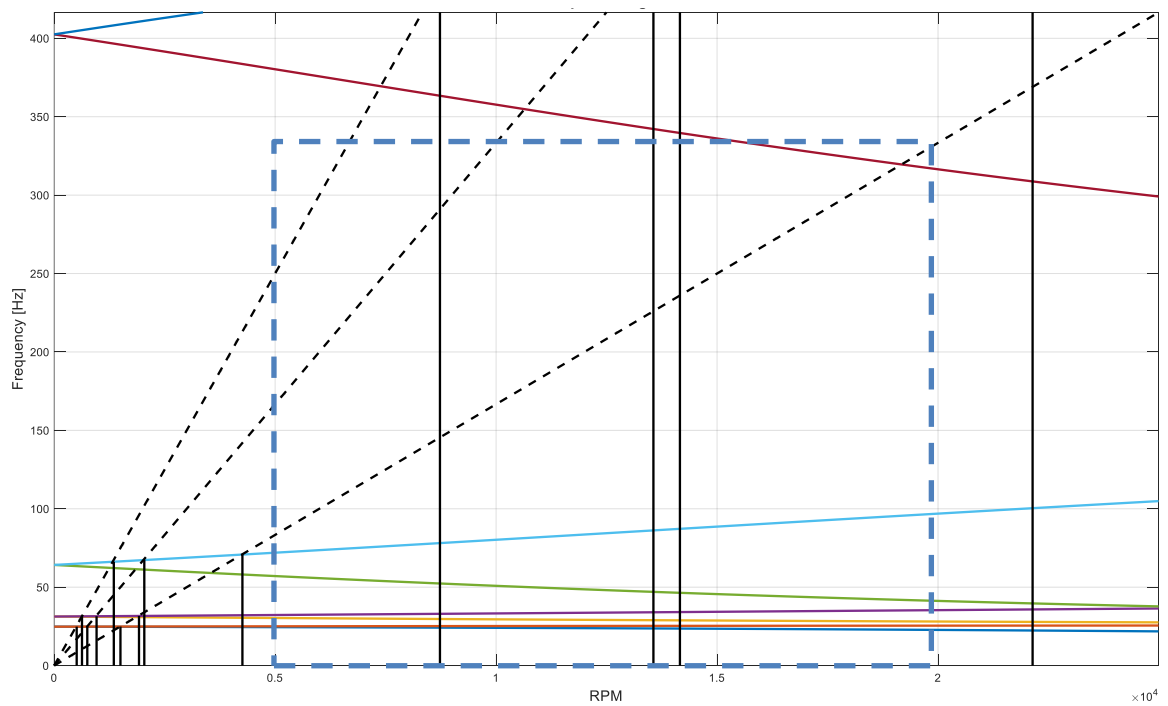


Figure 29. Campbell diagram of case study drivetrain with 46.5×50 mm thin shaft coupling.

With unbalance response analysis the amplitude of vibration at specific speeds can be seen. Analysis is performed with G 2.5 residual unbalance in impeller. Both shafts are modelled without unbalance. As calculation step 30 rpm has been used. Results of 46.5×122 mm thin shaft is presented in Figure 30. The vibration response in the operating range is small at any location (maximum vibration in commission phase was $80 \mu\text{m}$). The displacement values on both sides of the coupling are less than $1 \mu\text{m}$. However, it must be considered that displacements are on a different side of the center line as can be seen from Figure 31. From unbalance response analysis can be seen also high response at 25 830 rpm (max. $548 \mu\text{m}$). At that speed 1X cross the second flexible mode.

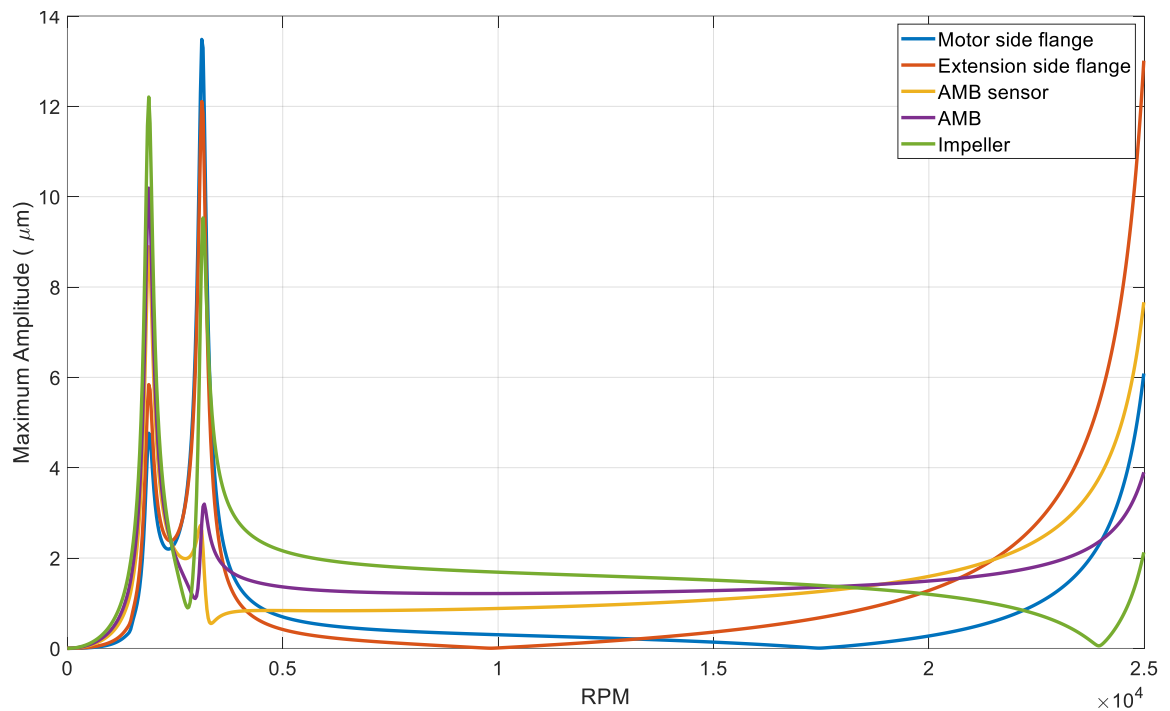


Figure 30. Unbalance response of case study drivetrain with 46.5×122 mm thin shaft coupling.

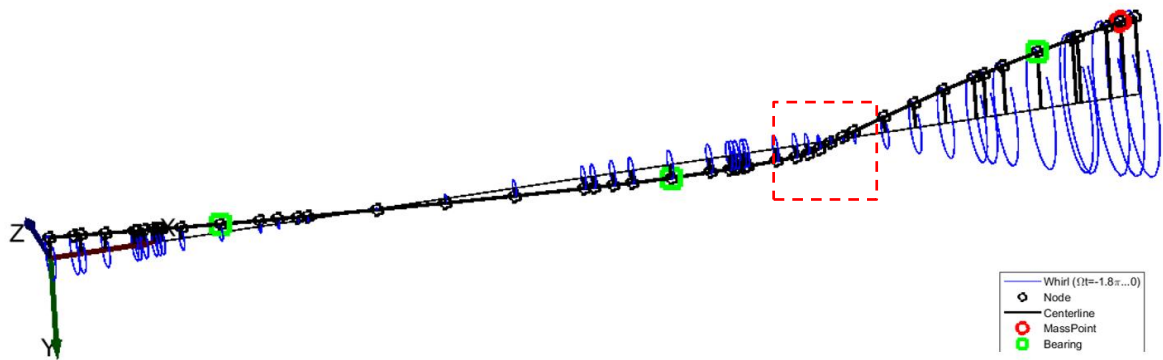


Figure 31. Whirling mode at 12000 rpm of case study drivetrain with 46.5×122 mm thin shaft coupling.

To understand the significance of the vibration at critical speed, an analysis of the resulting stresses has been performed. Table 12 shows the results of the analysis. The analysis is performed with Ansys 2021 R1 software. The displacement values from unbalance calculation are inserted in the model. Calculation is performed at the 1st flexible mode critical speed. Displacement in impeller location is $9.5 \mu\text{m}$ and $-13.5 \mu\text{m}$ in coupling left flange (deviation $23 \mu\text{m}$). Stress can be calculated also with equation 15. In equation 15, cross section over the length cannot change. Thus, the left and the right flange ($-12.1 \mu\text{m}$) displacement values (displacement difference over the coupling) have been used in calculation (deviation $1.38 \mu\text{m}$). Results are presented also with G71 unbalance class. With rated operation speed (12 000 rpm) stress in the coupling gets the value of 0.12 MPa.

Table 12. Case study drivetrain stress analysis in the thin shaft coupling at the 1st critical speed with G2.5 and G71 unbalance situations.

Configuration	1 st flex (rpm)	Deviation (μm) G2.5		Stress (MPa) G2.5		Deviation (μm) G71		Stress (MPa) G71	
		FEM	Eq. 15	FEM	Eq. 15	FEM	Eq. 15	FEM	Eq. 15
46.5 x 122	3120	23.0	1.38	1.5	1.4	400.6	24.85	26.4	24.5

3.4.4 Usability of disc coupling in drivetrain

The drivetrain model with disk coupling was created with RoBeDyn. The flange and spacer were modelled with beam elements. The flexible plate element was replaced with the previously analysed point stiffness values. Figure 32 shows the beam element model of disc

coupling. Point stiffness is located between nodes 40 and 41. The rest of the drivetrain is modelled as a same way than thin shaft configuration.

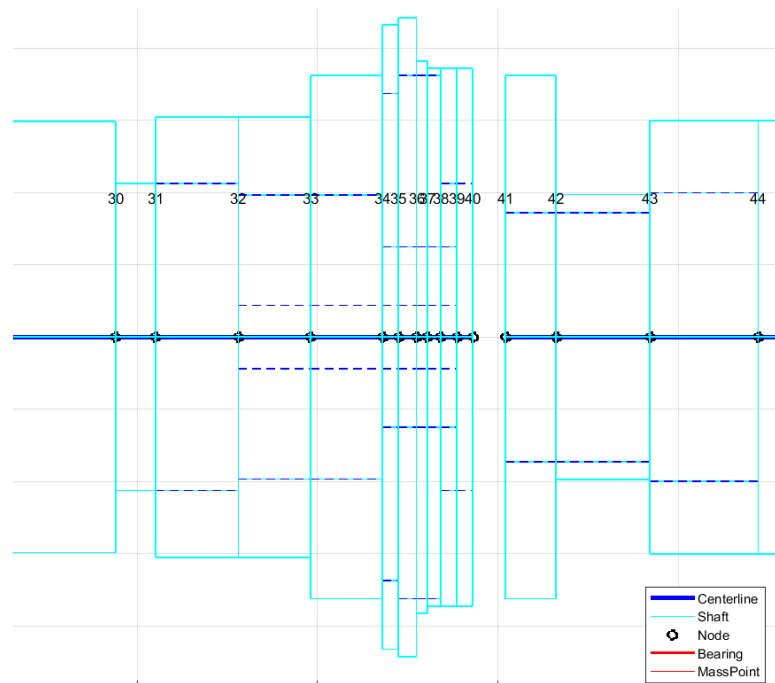


Figure 32. Disc coupling modelled with beam elements and point stiffness between nodes 40 and 41.

With the disc coupling the gap between the 1st and the 2nd flexible mode at zero speed is 362.5 Hz and is then 53.5 Hz wider than in the case of the 46.5 × 122 mm thin shaft. The 1st flexible mode gets only 23.9 Hz frequency. In the 2nd bending mode the drivetrain bends uniformly and can be said that shafts are dynamically heavily coupled. However, the 2nd bending mode natural frequency appears in 386.3 Hz with zero speed. This suggests that none of the 1X critical speeds are in the operation area, which can be confirmed from Campbell diagram from Figure 34. 2X and 3X critical speeds are in the operation range but not directly at rated speed. Mode shapes and nodal locations are presented in Figure 33.

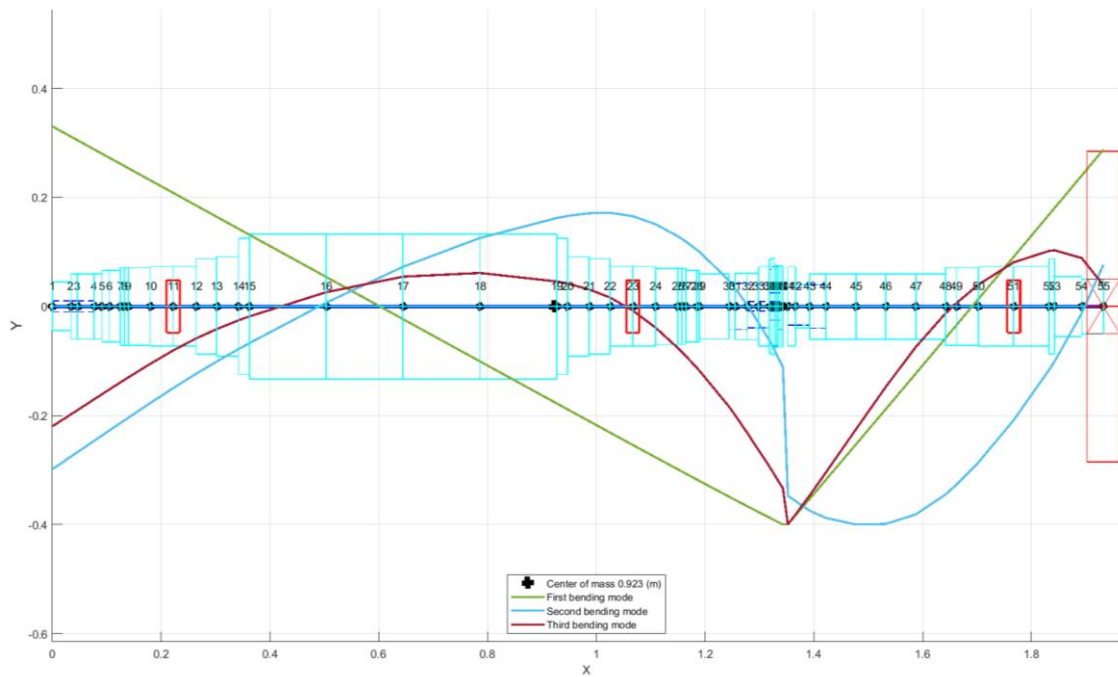


Figure 33. Free-free modes and frequencies of case study drivetrain with disc coupling.

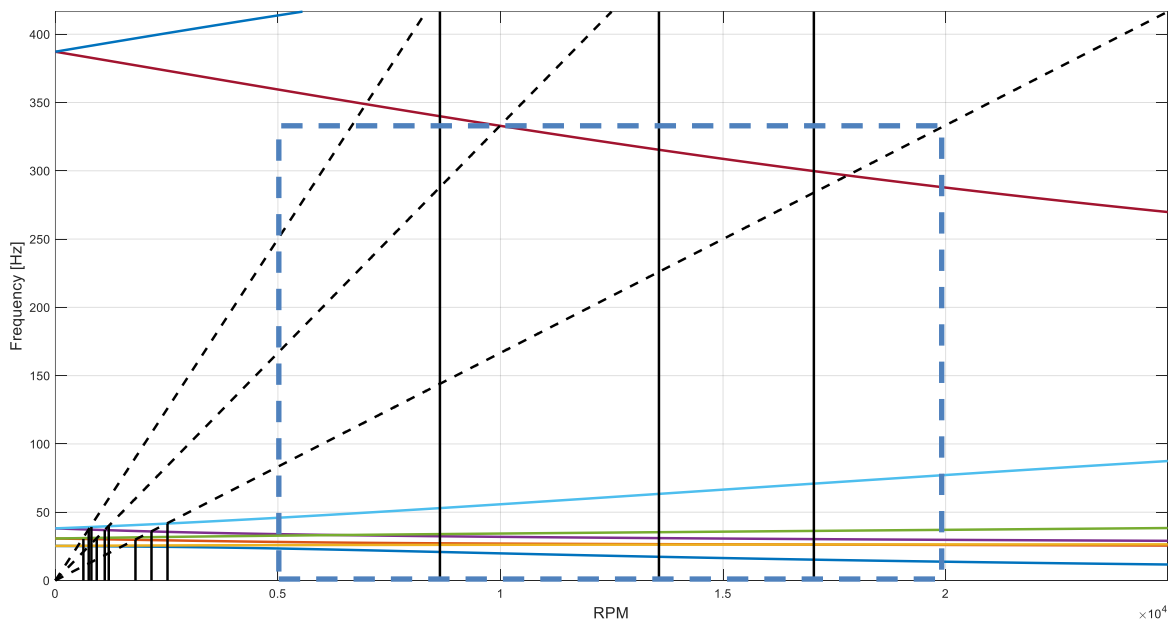


Figure 34. Campbell diagram of case study drivetrain with disc coupling.

The criticality of the crossing of the 1st flexible frequency was evaluated with unbalance response and stress analysis in the same way as for the thin shaft. The maximum amplitude of the 1st bending mode was half of the thin shaft reaching the 7 μm displacement. Figure 35 shows also that amplitude of 1st flexible is lower than the rigid mode amplitude.

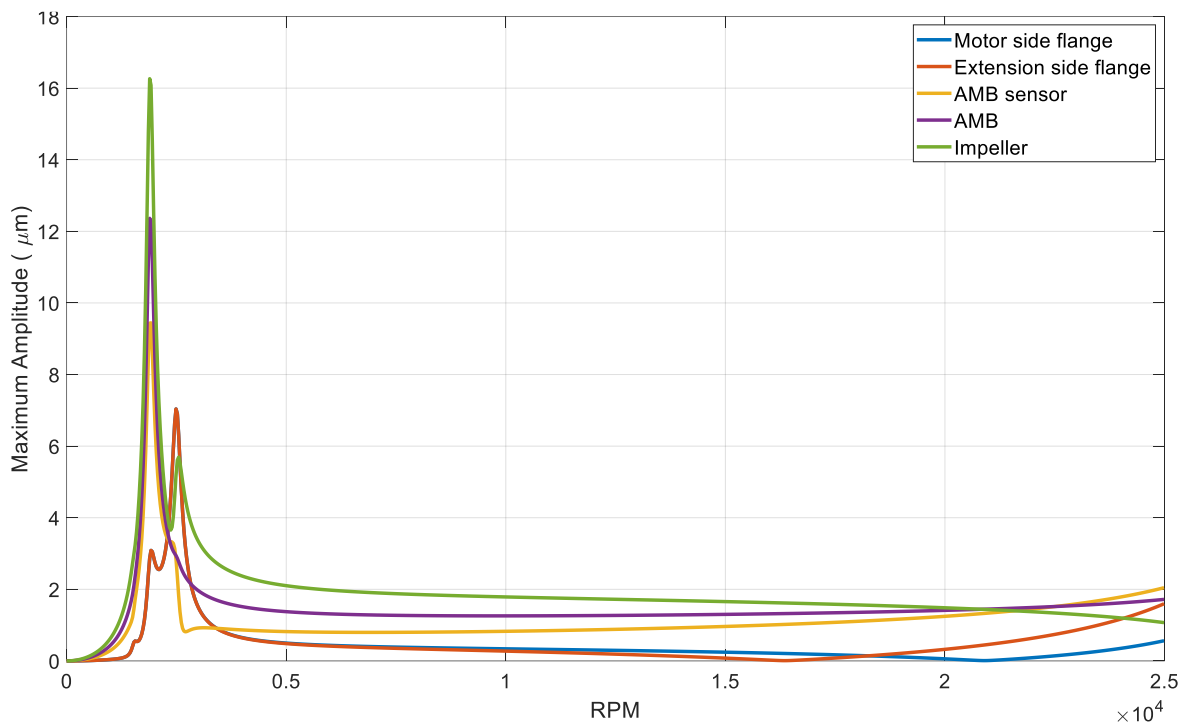


Figure 35. Unbalance response of case study drivetrain with disc coupling and G2.5 unbalance class.

Stresses from the crossing of the 1st critical speed was obtained to be on a low level, but lightly higher than with the thin shaft. With rigid modes significant bending does not occur over the drivetrain and thus no stress is generated. Table 13 present the result of the disc coupling stress analysis.

Table 13. Case study drivetrain stress analysis in the disc coupling in the 1st critical speed with G2.5 and G100 unbalance situations.

1 st flex (rpm)	Deviation (µm) G2.5	Stress (MPa) G2.5	Deviation (µm) G71	Stress (MPa) G71
2490	12.7	1.9	221.5	33.4

Whirling mode in the 1st flexible shows the bending happening in two planes (Figure 36). The same phenomenon appears also with the thin shaft but not as clearly as with the disc coupling. With both couplings the rated speed whirling mode emerge similarly as it is in Figure 31.

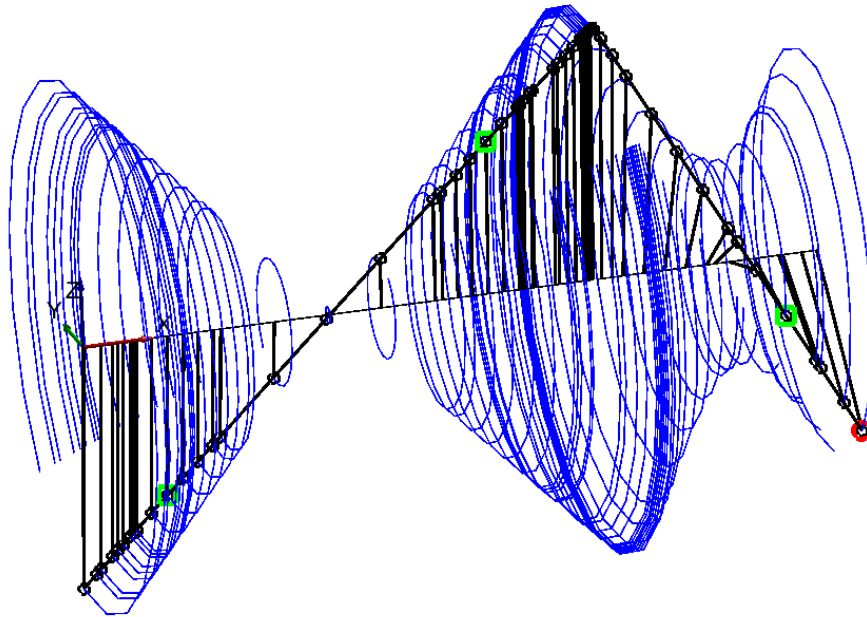


Figure 36. Whirling mode at 2490 rpm of the case study drivetrain with disc coupling.

3.5 Torsional and axial natural frequencies of thin shaft and disc coupling

Torsional and axial responses were analysed with software's capability to use solid elements. Analysis was performed with ANSYS R1 and SolidWorks 21 software. Modes below the 600 Hz were included in the analysis. Results are presented in Table 14.

Table 14. Drivetrain torsional and axial modes up to 600 Hz with the disc and the thin shaft coupling types.

Coupling type	Torsional		Axial	
	SolidWorks	ANSYS	SolidWorks	ANSYS
Thin shaft	83	75	535	534
Disc coupling	132	157	83	93

Axial mode appeared in both cases in the coupling but was more clearly visible directly in coupling with disc coupling case.

3.6 Analysing the results

Results are analysed for validation purposes. From baseline design, usage of cantilever beam equation combined with spring equation (equation 12) for calculating the required length of solid cylindrical baseline coupling is analysed by comparing the results with FE-method. Table 15 presents the results of FEM analysis for three thin shaft configurations based on

the baseline calculations (Table 5, case 1). Models were calculated to reach 20 μm displacement due to unbalance and gravitational forces. In FEM model the same radial force (256 N) located in extension shaft end of coupling was used. Rotor side was modelled as fixed to the rotor's end.

Table 15. Thin shaft displacement analyzed with FEM using the force calculated from 20 μm acceptable displacement with baseline drivetrain configuration with G2.5 residual unbalance (Table 5, case 1).

Thin shaft	Displacement FEM (μm)	Deviation (%)
58.5 x 296.5	23.9	16.3
46.5 x 218.3	23.1	13.4
42 x 190.6	22.8	12.3

To evaluate the results of drivetrain analyses, the disc coupling, and the 46.5 \times 122 thin shaft coupling were analysed using the FEM with solid elements. Results of free-free frequency analysis and deviation compared to the RoBeDyn beam element model are presented in Table 16.

Table 16. Free-free frequencies [Hz] of drivetrain analysis with the disc and 46.5 \times 122 thin shaft coupling.

Mode	SolidWorks	ANSYS	RoBeDyn	Deviation (%)	
				Sol. / RoB.	ANS. / RoB.
Disc, 1 st flex.	11	27	24	52	13
Disc, 2 nd flex.	294	324	386	24	16
Disc, 3 rd flex.	452	571	685	34	17
Thin, 1 st flex.	38	37	39	2	6
Thin, 2 nd flex.	307	302	348	12	13
Thin, 3 rd flex.	489	535	612	20	13

4 DISCUSSION

Discussion is divided in three sub-chapters. The first chapter discusses the usability of the three AMB configuration. The second chapter studies the coupling design and lastly what was missed from this study and should be then studied in the future.

4.1 Usability of three AMB drivetrain

To be able to produce a high-speed electric machine in megawatt range in serial production it is needed to find a way to use various impellers with the same electric machine. To solve this problem an arrangement where impeller is attached on an additional extension shaft which can be tuned for any individual compressor or turbine is proposed. The research hypothesis was that a flexible coupling between rotor and extension shaft enables a situation where the rotor dynamics of the electric machine does not change due to different impellers on the additional shaft and thus any physical changes are not needed in the electric machine.

Results from chapter 3.4.1 where stiffness effectiveness was analysed in the case study drivetrain show that with stiffness values below $1 \cdot 10^5$ (bending) Nm/rad and $1 \cdot 10^6$ (radial) N/m a situation is created where rotor's vibration responses act as individual components. By increasing the stiffness, the natural frequencies of the system start to go higher and modes behave as one body. After the values $1 \cdot 10^8$ Nm/rad and $1 \cdot 10^{10}$ N/m higher stiffness does not affect the results. The effect of increasing stiffness can be seen as similar behaviour from Corcoran et al. (2007) study of coupling support stiffness analysis and Kleynhans et al. (2005) study of bearing stiffness evaluation.

By using the stiffness values below $1 \cdot 10^6$ (radial) N/m in coupling opens the possibility where different impellers attached to the extension shaft does not affect the electric motor's rotor dynamic. The possible problem related to the confirmed hypothesis was stated in the beginning of the work to be stability of the three AMB system with the low coupling stiffness.

With static equilibrium analysis the required radial stiffness in the coupling to handle the unbalance and gravitational forces was evaluated. In the case study configuration minimum

radial stiffness required from the coupling was $1.39 \cdot 10^7$ N/m. From the results it can be seen that changes in impeller mass, unbalance and extension shaft dimensions have a high effect on the required stiffness. Thus, it can be stated that the required radial stiffness for various usages is in the level of $2 \cdot 10^8$ N/m with the case study configuration. Combining the result of static equilibrium analysis and stiffness evaluation can be said that a totally dynamically uncoupled drivetrain cannot be build. To be able to ensure stability of the system radial stiffness needs to be at such a level that rotor dynamics are also coupled. However, by designing the right stiffness values for the coupling can be created wide operation range without critical speeds.

It was observed that coupling bending stiffness affects considerably only the bow type bending mode (the first bending mode of a straight body) and its frequencies. Radial stiffness affects the S- shape mode, which is the straight body's second bending mode, but not the bow type bending mode. Radial stiffness affects also the 3rd and 4th modes of the drivetrain. Thus, to create a wide operation range, radial stiffness is required to be high and bending stiffness as low as possible. With this combination operation range between drivetrain's 1st and 2nd flexible modes can be created.

It was also observed that the rotor's and extension shaft's individual 1st bending modes generate drivetrain's 3rd and 4th bending modes. When radial stiffness increases over the level of $1 \cdot 10^6$ N/m, the 3rd mode appears in shapes as a double bow in the same direction. The 4th mode shaft, which has lower individual bending mode, appears in S- shape and other shaft in bow shape. Natural frequencies of the 3rd and 4th modes start from the individual shaft's 1st bending frequencies with a low coupling stiffness and go higher when the stiffness is raised. This means in terms of design and operation that the natural frequency of the electric motor's rotor must be higher than the operating speed. As can be seen in Figure 21 rotor's individual bending mode frequency is 796 Hz, which is considerably higher than what rotor can handle centrifugal forces. This allows for a lower bending mode of the rotor compared to integrated solutions where the rotor frequency is reduced by the impeller. This phenomenon can be useful in rotor design e.g., in electric design perspective. However, lowering the individual component's natural frequency will lower also the 2nd drivetrain mode frequency with high correlation.

From the case study drivetrain was observed that the 2nd mode free-free frequency is about $0.5 \times 3^{\text{rd}}$ mode free-free frequency (Individual 1st bending mode of impeller attached to the extension shaft). Changes in the impeller mostly affect the frequency of the 2nd mode. However, changes in impeller do not have so big effectiveness than in an integrated construction as can be seen in Figure 37. The figure compared the case study rotor as an integrated and as a dual-shaft (rotor + extension shaft) version with 40 mm width solid steel disc. Exact frequencies are depending on the attachment type etc. but effectiveness of changes in impeller can be seen in the figure.

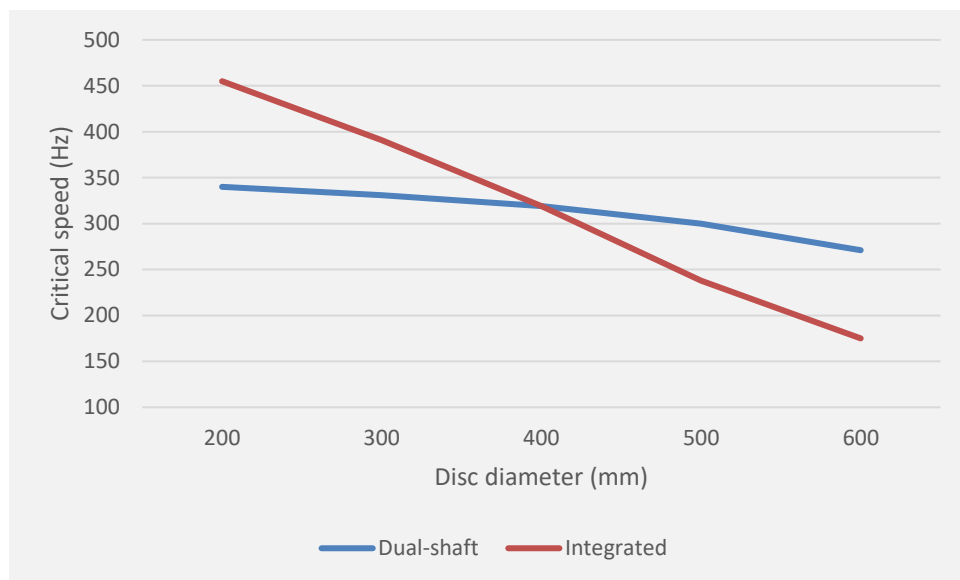


Figure 37. Comparison of case study rotor as integrated construction and with extension shaft using a 40 mm width solid steel disc.

When moving to higher power categories it requires a higher impeller area if surface velocity is kept as a constant (strength of materials are limiting factor for surface velocity (Budynas & Nisbett 2015)). Due to larger impeller, rotational velocities cannot be kept as high when moving into higher powers. Phenomenon can be seen from table presented by Poso (2019, p.50). Higher power requires also larger active part for the rotor, larger active part requires more force from AMBs which results larger area of AMB. At some point it may not be convenient anymore to attach an impeller onto the rotor. However, from literature and market can be seen cases up to the 8 MW induction machines in gas compression applications when AMB supported rotor has been used as integrated solution (Gilon &

Boutriau 1998). So, it can be said that rotor could be designed in multimegawatt range as integrated solution when it is designed for a specific application. However, about combining the higher load capacity of three AMBs to wider operation range with heavier impellers it can be concluded that the extension shaft solution may offer a possibility to utilize so called standard high-speed electric motor in megawatt range. In the future, the most suitable operation areas, and usability of the integrated, three-bearing and four-bearing versions should be studied closely. The target should be to figure out when different bearing configurations are most beneficial and even possible.

4.2 Coupling in the three AMB drivetrain

With the proposed coupling design method, it was possible to create a model which theoretically works as a coupling. Analytical calculations were found to be a quick way to design baseline model for coupling. Only a few initial requirements were used as starting values (power, speed, radial displacement, material parameters) to create the results. Required radial stiffness were estimated to be critical calculation step. Analytical calculation results were compared with the FEM results and were found to be accurate enough. The biggest question mark in the calculation was the real required radial stiffness. In the calculations dynamic factor (4) was used for maximum displacement. Due to high angular velocity and gyroscopic effect, it may be the case that factor 4 is too high. On the other hand, dynamics of three AMB system is unclear and possible misalignment can cause excessive vibration if coupling location is not supported with high radial stiffness. The rapid dynamic analysis method for three AMB solution would be critical to develop when studies continue.

From initial requirement it was found that the static transient torque-based design is including also fatigue capacity. In the baseline design only the torque load fluctuation was used. Result of stress analysis could be used to evaluate fatigue life against bending loads, but it was left out of scope in this work. And it must be noted that those results do not contain the possible misalignment which can generate a high loading in the coupling. For later stress analysis is important to utilize results of drivetrain control analysis. From those results loading cycles over the time (e.g., rump-up loads) can be implemented and thus obtain more accurate fatigue calculations.

Dynamic analyses were performed with a beam element model to speed up the calculation. The results were compared to a solid element model implemented with two different commercial software. Deviation of results were found to be in same level than in similar cases in the literature (6-17 % (Hz)). With the thin shaft configuration where coupling geometry can be modelled with beam elements, the difference in the first mode between the beam and the solid elements was 6%. In paper presented by Kurvinen et al. (2021a) where the case study original rotor was experimentally tested, the difference between the beam model and the experimentally tested values was to be found to be 5.4% (Kurvinen et al. 2021a). In introduction section it was told the study of Bydynas & Nisbett (2015) where beam and solid element model difference in first bending mode was 1.6%. However, the structure of the study was much simpler.

With the disc coupling, variation in the results was found to be more than in the thin shaft case. Difference between Ansys and the RoBeDyn results was to be found less (13%) than the difference between the RoBeDyn and the SolidWorks (52%). The reason behind this is probably in point stiffness values used in RoBeDyn analysis which was analysed with Ansys software. The disc coupling includes many parts and a lot of attachments, so differences cannot be avoided. It is important to continue the study and obtain the experimental results to validate and verify the method and models used with disc coupling. Study presented by Corcoran et al. (2007) which compared different analysis method with disc coupling. In their study the difference in the first bending mode between the methods was ~ 16%.

In general, the results appear to be useful in terms of reliability. The only difference from previous studies was found in the analysis of disc coupling stiffness values. Zhao et.al. (2016) stated in their work that torsional stiffness values are not constant in relation to load. No variability was observed in the results of this study. Difference in stiffness values with the same torsional load between the studies was 39%. In the Zhao's study, the difference in the stiffness values were much higher between the load cases. The reason for constant values in this study may be due to discs structure in analysis, 3D model obtained from manufacturer does not consist separate disc plates in flexible element, it was modelled as a one piece. The nonlinearity of the displacement when loading a plate-like structure perpendicular to its plane is a well-known phenomenon (Timoshenko 1983). This can be an explanatory factor for the nonlinearity of the disc coupling. One possible room for error may be too big mesh

size. So, nonlinearity is likely to exist in a disc coupling, but it was not found in this study. Its effectiveness should be investigated as the study continues.

4.2.1 Key findings of commercial couplings

Low bending stiffness was found in all the commercial couplings investigated in this study. Low or zero bending stiffness is related to the need of capability to handle angular misalignment, which is a required feature of flexible couplings. Most of the commercial couplings were not able to satisfy the required speed of the drivetrain. The reason for lack of top speed may lie in the structure of coupling and materials used to create the flexibility. In jaw-type coupling elastic material to transfer the torque is used. Such material probably cannot stand a high centrifugal force. Couplings where joints are used to transfer torque with zero bending stiffness includes structure where clearances may cause high vibration at a high speed. One possibility for low top speed may be their capacity to transfer torque with high angle between shafts. For example, Rzeppa- type coupling could be one possible solution for high-speed operation with low misalignment. However, even it could handle high speeds wear in balls could be a problem or downside from maintenance point of view.

Special purpose couplings, determined in ISO 10441 are the only coupling type group which is commonly usable in high-speed applications. From that group disc coupling was found to be the most suitable for the case study purpose. The disc coupling used in analysis contains a low bending and high radial stiffness. It offers a wide operation range between the 1st and the 2nd critical speeds, with a low response when crossing the first critical. Downsides of disc coupling can be stated to be lack of axial load capacity. With a disc coupling the extension shaft should be equipped with an axial bearing. Due to low axial stiffness, a drivetrain also generates easily axial vibration modes below the rated operation speed. In the case study axial frequency was just out of the safety margin in lower end of operation range.

4.2.2 Key findings of baseline couplings

From baseline values the thin shaft coupling model was created. In this case the dynamic response of the drivetrain was similar to the disc coupling case. The bending stiffness of the thin shaft solution could not be designed at the same level as the disc coupling and thus the

first mode occurs at a higher level. Frequency is nevertheless out of operation range with high safety margin. A good feature of the thin shaft is its high axial stiffness. Due to that, it is easier to design a drivetrain's axial mode out of the operation range. High axial stiffness also enables to transfer axial loads. At its simplest, the thin shaft consists of only one part, attached with an interference fit. That will provide a low manufacturing cost and reduce the possibility of errors. The thin shaft usability also includes a possibility to install it through an impeller, which allows impeller attachment at both ends of the extension shaft.

Hollow cylindrical version could have been created also from the baseline values. However, a bellows coupling follows similar structure, and it was evaluated within commercial alternatives. In a commercial Bellows coupling the radial stiffness was not at a sufficient level. This is probably due to the need for the coupling to handle the parallel misalignment in four bearing cases, which is not required in a 3 AMB system and thus hollow coupling can be put list of future studies. It was mentioned in the results that with hollow cylindrical shape the wall thickness based on minimum torsion load capacity may lead a solution when other failure criteria (buckling) than yielding may take place (Timoshenko 1983). In a bellows coupling the outer surface is designed with a wave shape which provides rigidity against local deformations but does not prevent the radial deflection or bending. This method could be used if a hollow type coupling is designed for a 3 AMB drivetrain.

4.3 In scope of future studies

A few general topics for future research have been already mentioned in the discussion. The more specific topics related to suitable coupling design are discussed next. When is compared two designs presented in this work (thin shaft, disc coupling) can be said that disc coupling was able to generate wider operation range between 1st and 2nd modes. Also, nodal locations appear in better spots from controllability point of view (further away from the sensor and bearing). It is still impossible to say that is it a common feature or just a case of this configuration. With analysis of different impeller configurations could be answered for this question.

Damping is one major feature on field of machine dynamics. It can be used to decrease the vibration amplitude in the system. Damping possibilities in the coupling was not included into this work. It may be difficult to design damping properties and high rigidity for high

speed at the same time. This can be seen e.g., from jaw coupling where has damping capability due to elastic material between the jaws but no products for high-speed with high torque capacity. The need of damping properties becomes clearer after the effectiveness of 1X backward, 2X and 3X radial and torsional vibration will be investigated. As it was previously mentioned angular misalignment may excite rotational speed harmonics. Torsional excitation is related heavily to impeller and its behavior in use. Torsional and rotational speed harmonics can be major cause of fatigue failure in the coupling (Locke et al. 2013). When the system is experimentally tested and verified, studies can focus more to answer fatigue in long term usage. In disc coupling can be said to include good properties from failure safety point of view due to its laminated disc structure. Failure of one disc lamination may not cause total failure of coupling but in thin shaft solution fatigue failure may not be seen before the total failure of coupling. The capability of the AMBs to dampen the vibration is one major factor in coupling deflection and thus its fatigue life. The damping properties in this study were based on old studies that need to be updated in future.

Attachment of the couplings was not deeply under study in this work. Rigid attachment type used with flexible element may reduce importance of precise values in attachment (torque transferring capacity will provide necessary rigidity in coupling). But that is fully on hypothesis level, which should be investigated before the experimental studies are performed. It is also good to know how much attachment rigidity affects the natural frequencies of a system and is there a clear boundary when its effectiveness will start to be significant.

Maybe the most important aspect of future studies is to build a control model for AMBs. It is necessary for experimental test of drivetrain which is the starting point of final step of whole three AMB extension shaft idea and as well as the coupling research. With a control algorithm (similarly as what is made in this study) the effectiveness of coupling support stiffness to displacement of drivetrain can be tested. If the control analysis results correspond to this study results, proposed coupling configuration can be implemented in real life test setup. The control results and results of this study can be used to validate results of each other. Differences and similarities in the results can be used to develop design method presented in this work e.g., usability of dynamic factor in calculations. The control algorithm is also the key tool to test how the drivetrain will behave with different impellers on it.

5 CONCLUSION

This work has studied high-speed electric machine drivetrain properties in megawatt power range. The real-life problem behind the work is found from the difficulty to implement high-speed machines for various purposes. To solve this problem the solution has been stated to be as; With a flexible element between the electrical machine rotor and working device impeller a situation can be arranged where electric motor's rotor can be built in a way that there is no need to make physical changes when different impellers are attached on the drivetrain. The key feature to accomplish the statement lies in the rotor dynamics. With a flexible element, rotor natural frequencies and their mode shapes do not change significantly with different impellers. The problems related to the solution were identified to be ability to transfer high torque at high speed with a flexible element.

Baseline calculation method for the flexible element i.e., coupling design was implemented. With the method it was possible to rapidly calculate baseline values from initial requirements (power and speed). From literature a few restrictions were obtained to set boundaries for the design (transient torque, safety margins, maximum displacements, material parameters, etc.). From the baseline values a thin shaft solution was created. It consists only of a solid circular shaft where the diameter and length are calculated to match torque, speed and required radial stiffness (to maintain the coupling displacement at a limited value). Commercial coupling possibilities were evaluated, and disc coupling was found to fulfil the initial requirements and it was selected on drivetrain analysis.

Using dynamic analysis it was evaluated in the first place how the drivetrain dynamic behaviour changes in relation of different point stiffnesses between the rotor and the extension shaft (shaft for impeller attachment). From the results it could be seen that there are two bending and radial stiffness combinations which could fulfil a wide range of operation with the drivetrain. The first combination with a wider operation range where both radial and bending stiffnesses are in a low level was found to be impossible to implement in terms of the radial support obligation of the coupling. The second combination where radial stiffness is as high and bending stiffness as low as possible was observed to be possible to be implemented with the baseline coupling and with the disc coupling.

When both coupling candidates offer the desired operation range, differences can be found mainly from the usability. The good features of disc coupling are its capability to handle angular and axial misalignment, high radial stiffness and structure to avoid total failure in fatigue situation. Two downsides of disc coupling are its complexity which can be seen from the price and its lack of axial load capacity. Both disc coupling cons can be found from pros features in thin shaft coupling. The small diameter of the thin shaft can also be mentioned as its good feature, it allows e.g., the thin shaft to be installed inside a rotor and the extension shaft. The cons of thin shaft can be found from its sensitivity for fatigue loading.

The aim of the study was to clarify whether a three-bearing system is feasible to implement or not and how it can be executed at preliminary stage. A lot of additional research will be needed, the most important of it is the development of a control algorithm for the 3 AMB drivetrain. The results of this study can be used as a starting point for control design and results from those analyses can be used to develop a design method and coupling design itself. Combining the design steps of the coupling, rotor and control it is possible to optimize the rotor to operate with the widest possible range of impellers without need to make changes in the electrical machine.

LIST OF REFERENCES

- Access-energy, 2022. Technologies. [Access Energy webpage]. [Accessed 2 January 2022]. Available at: <https://access-energy.com/tech.html>
- Biolini, A., 2007. Reliability Engineering, Theory and Practice. 5th edition. Pringer-Verlag Berlin Heidelberg. 593 p.
- Budynas, R., G., Nisbett, K., 2015. Shigley's Mechanical Engineering Design. 10th edition. McGraw-Hill. New York. 1082 p.
- Choudhury, T., Kurvinen, E., Sopanen, J., 2019. Model Based Unbalance Identification for Paper Machine's Tube Roll. In IFToMM World Congress on Mechanism and Machine Science. Springer, Cham, pp. 3375–3384
- Chen, Z., Y., Zeng, Y., 2006. Classification of Product Requirements Based on Product Environment. Concurrent Engineering: Research and Applications, SAGE Publications, 14 (3), pp. 219–230.
- Childs, P., 2014. Mechanical Design Engineering Handbook. Chapter 19 - Engineering Tolerancing, pp. 761–769.
- Corcoran J., Lyle, D., McCormack, P., Ortel, T., 2007. Advanced in Gas Turbine Couplings. Proceedings of the Thirty-Sixth Turbomachinery Symposium, pp. 157-172.
- Dumitru, N., Secară, E., Mihalcica, M., 2009. Study of Rotor-Bearing Systems Using Campbell Diagram. Proceedings of the 1st International Conference on Manufacturing Engineering, Quality and Production Systems, 2, pp. 393–396.
- Eskelinen, H., Karsikas, S., 2013. DFMA-opas: Valmistus- ja kokoonpanoystävällisen tuotteen suunnittelu. Lappeenranta: Lappeenranta University of Technology. 115 p.
- Feehally, T., 2012. Electro-mechanical interaction in gas turbine-generator systems for more-electric aircraft. The University of Manchester (United Kingdom). 304 p.
- Fenner drives, 2012. Keyless locking devices. [web document]. [Accessed 28 October 2021]. Available at: <https://docs.rs-online.com/d2e1/0900766b8113c78d.pdf>
- Gardner Denver, 2021. Energy and vacuum systems, turbo blowers. [Gardner Denver webpage]. [Accessed 19 November 2021]. Available: <https://www.gardnerdenver.com/en-qa/runtech/energy-and-vacuum-systems/turbo-blowers>
- Gerada, D., Mebarki, A., Brown, N. L., Gerada, C., Cavagnino, A. & Boglietti, A., 2014. High-Speed Electrical Machines: Technologies, Trends, and Developments. Transactions on Industrial Electronics, 61.6, pp. 2946–2959.

Global Industry Analysts Inc, 2020. Industrial gearbox - global market trajectory & analytics. 713 p. & Global Industrial Solution High-Speed Motor Industry Market Research Report. 124 p. Not available in public.

Gilon, D. C., & Boutriau, L., 1998. Experience With High Speed Induction Motors For Direct Driving Of Compressors. In Proceedings of the 27th Turbomachinery Symposium. Texas A&M University. Turbomachinery Laboratories. 5 p.

Grönman, A., ... 2020. Design and verification of a hermetic high-speed turbogenerator concept for biomass and waste heat recovery applications. *Energy Conversion and Management*, 225. 13 p.

Guskov, M & Sinou, J.-J., & Thouverez, F., & Naraikin, O., 2007. Experimental and Numerical Investigations of a Dual-Shaft Test Rig with Intershaft Bearing. *International Journal of Rotating Machinery*. 12 p.

ISO 10437 2003. Petroleum, petrochemical and natural gas industries - Steam turbines - Special-purpose applications. 2nd. edition. Genève: International Organization for Standardization. 113 p.

ISO 10441. 2007. Petroleum, petrochemical and natural gas industries. Flexible couplings for mechanical power transmission. Special-purpose applications. 56 p.

ISO 14839-2. 2004. Mechanical vibration – Vibration of rotating machinery equipped with active magnetic bearings – Part 2: Evaluation of vibration. 1st. edition. Genève: International Organization for Standardization. 20 p.

ISO 21940-11. 2017. Mechanical vibration. Rotor balancing. Part 11: Procedures and tolerances for rotors with rigid behaviour. Genève: International Organization for Standardization. 20 p.

Jin, C., Xu, Y., Zhou, J., & Cheng, C., 2016. Active magnetic bearings stiffness and damping identification from frequency characteristics of control system. *Shock and Vibration*. 8 p.

Johnson Power LTD. 2021. Products. [Johnson Power webpage]. [Accessed 18 November 2021]. Available: <https://www.johnsonpower.com/products/>

Kleynhans, G., Pfrehm, G., Berger, H., & Baudelocque, L., 2005. Hermetically Sealed Oil-Free Turbo compressor Technology. In Proceedings of the 34th Turbomachinery Symposium. Texas A&M University. Turbomachinery Laboratories, pp. 63–76.

Kurvinen, E., C., Petrov, I., Nerg, J., Liukkonen, O., Jastrzebski, R., Kepsu, D., Jaatinen, P., Aarniovuori, L., Sikanen, E., Pyrhönen, J., Sapanen, J., Pyrhönen, O., Niemela, M., Kangasmaki, T., 2021a. Design and Manufacturing of a Modular Low-Voltage Multi-Megawatt High-Speed Solid-Rotor Induction Motor. *IEEE Transactions on Industry Applications*, pp.1–10.

Kurvinen, E., Choudhury, T., Narsakka, J., Martikainen, I., Sapanen, J., & Jastrzebski, R. P., 2021b. Design Space Method for Conceptual Design Exploration of High Speed Slitted

Solid Induction Motor. In 2021 IEEE International Electric Machines & Drives Conference (IEMDC), pp. 1-8.

Lalanne, M., Ferraris, G., 1998 Rotordynamics prediction in engineering. John Wiley & Sons. 252 p.

Lee, K., H., Park J., E., Kim Y., K., 2019. Design of a stiffness variable flexible coupling using magnetorheological elastomer for torsional vibration reduction. Journal of Intelligent Material Systems and Structures 1–10. 10 p.

Locke, S., R., Burgess, M., J., Corcoran, J., P., Hess, T., D., coupling credible failure modes and owner options to intervene. Forty-Second Turbomachinery Symposium. Houston, Texas. 29 p.

Logan, D., L., Chaudhry K., K., 2012. A First Course in the Finite Element Method. 5th ed., Cengage Learning. 925 p.

Lovejoy-inc. 2021. Products. [Lovejoy-inc webpage]. [Accessed 18 November 2021]. Available: <https://www.lovejoy-inc.com/products/>

Man Energy Solutions, 2021. Process industry, products, compressors, vacuum-blowers. [Man Energy Solutions webpage]. [Accessed 19 November 2021]. Available: <https://www.man-es.com/process-industry/products/compressors/vacuum-blowers>

Mobius Institute, 2021. Vibration analysis dictionary. [Mobius Institute webpage]. [Accessed 29 November 2021]. Available at: <https://www.mobiusinstitute.com/vibration-analysis-dictionary/>

Musgrove, G., Bauer, B., Hall, K., Hinchliff, M., Meher-Homji, C., Kurz, R., Pettinato, B., Ristanovic, D., Taher, M., 2019. Chapter 7 – Drivers. Compression Machinery for Oil and Gas. Gulf Professional Publishing, pp. 309–372.

Narsakka, J. (2020). Vibration measurement of high-speed electric motor post-assembly testing. 53 p.

Norelem. 2021. Products. [Norelem webpage]. [Accessed 19 November 2021]. Available at: <https://www.norelem.com/us/en/Products/Product-overview/Systems-and-components-for-machine-and-plant-construction/23000-Couplings-Rigid-couplings-Conical-clamping-rings-Cardan-joints-Quick-fit-couplings-Bearings/Shaft-hub-clamping-sets/23360-Keyless-locking-couplings-Form-G-increased-tolerance-range.html>.

Norton, R., L., 2006. Machine Design An Integrated Approach. 3rd ed., Pearson Education Inc. USA. 984 p.

NTN Corporation, 2021. Product & Technology. [NTN Corporation webpage]. [Accessed 19 November 2021]. Available: <https://www.ntnglobal.com/en/index.html>

Pahl, G., Beitz, W., Wallace, K., 1996. Engineering design: A systematic approach. 2nd ed., [enl. and updated]. London: Springer. 544 p.

- Pilkey, W., D., 1997. Peterson's stress concentration factors. 2nd ed., John Wiley & Sons, Inc. USA. 457 p.
- Poso, P. (2019) Startup Survival in B2B Markets: case ASynRo. 115 p.
- Pyrhönen, J., Nerg, J., Mikkola, A., Sopanen, J., Aho, T., (2009). Electromagnetic and mechanical design aspects of a high-speed solid-rotor induction machine, pp. 35-49.
- RENK-group, 2021. Products and service, couplings. [RENK-group webpage]. [Accessed 19 November 2021]. Available: <https://www.renk-group.com/en/home/>
- Regal Rexnord, 2021. Products, Couplings. [Regal Rexnord webpage]. [Accessed 19 November 2021]. Available: <https://www.regalrexnord.com/>
- RW Couplings, 2021. Products. [RW Couplings webpage]. [Accessed 19 November 2021]. Available: <https://www.rw-couplings.com/>
- Rivin, Eugene., I., 1999. Stiffness and Damping in Mechanical Design. Marcel Dekker Inc. New York, USA. 528 p.
- Santora, M., 2021. Should I choose a keyed or keyless coupling for this application. [Couplingtips webpage]. [Accessed 21 November 2021]. Available at: <https://www.couplingtips.com/featured/choose-keyed-keyless-coupling-application/>
- Sawalhi, N., Ganeriwala, S., Tóth, M., 2019. Parallel misalignment modeling and coupling bending stiffness measurement of a rotor-bearing system. Applied Acoustics, 144, pp.124–141.
- Scheffer, C., Girdhar, P., 2004. Practical machinery vibration analysis and predictive maintenance. Elsevier. 252 p.
- Srinivas, R., S., Tiwari R., Kannababu, C., 2018. Application of active magnetic bearings in flexible rotordynamic systems – A state-of-the-art review. Mechanical Systems and Signal Processing, 106, pp. 537–572.
- The Switch, 2021. High-speed motor and drive packages. [Accessed 10 December 2021]. Available at: <https://theswitch.com/turbo/motor-and-drive-packages/>
- Timoshenko, S., Woinowsky-Krieger, S., 1983. Theory of plates and shells. 2. ed., 24. pr. Tokyo: McGraw-Hill. 580 p.
- Tollok, 2003. Locking Assemblies. [web document]. [Accessed 19 Nov 2021]. Available at: https://www.movetec.fi/images/pdf/Tollok_catalogue.pdf
- Wayzone, N., D., Tupkar, A., B., 2012. Customization of catia V5 for Design of Shaft Coupling. Internationat Journal Of Computer Applications, pp.30–33

Wahl., A. M., Kilgore., L., A., 1940. Transient Starting Torques in Induction Motors, in Transactions of the American Institute of Electrical Engineers, 59, no. 11, pp. 603–607

Zhang, J., Zhang, H. H., He, Y. L., & Tao, W. Q. (2016). A comprehensive review on advances and applications of industrial heat pumps based on the practices in China. Applied Energy, 178, pp. 800–825.

Zhao, B., Zhao, Y., Feng, J., Peng, X., 2016. Numerical and experimental investigation of the torsional stiffness of flexible disc couplings. International Journal of Mechanical Sciences, 114, pp. 207–216.

RENK coupling stiffness analysis

APPENDIX I

Load	Moment (Nm)	Displacement (mm)	Rotation (rad)	Stiffness (Nm/rad)
Bending	10	$1,17 \cdot 10^{-2}$	$8,26 \cdot 10^{-5}$	$12 \cdot 10^4$
	50	$1,2 \cdot 10^{-2}$	$8,3 \cdot 10^{-5}$	$12 \cdot 10^4$
	100	$5,9 \cdot 10^{-2}$	$4,1 \cdot 10^{-4}$	$12 \cdot 10^4$
	150	$1,2 \cdot 10^{-1}$	$8,3 \cdot 10^{-4}$	$12 \cdot 10^4$
	200	$1,8 \cdot 10^{-1}$	$1,2 \cdot 10^{-3}$	$12 \cdot 10^4$
Torsion	10	$5,1 \cdot 10^{-4}$	$3,6 \cdot 10^{-6}$	$280 \cdot 10^4$
	50	$2,5 \cdot 10^{-3}$	$1,8 \cdot 10^{-5}$	$280 \cdot 10^4$
	100	$5,1 \cdot 10^{-3}$	$3,6 \cdot 10^{-5}$	$280 \cdot 10^4$
	150	$7,6 \cdot 10^{-3}$	$5,4 \cdot 10^{-5}$	$280 \cdot 10^4$
	200	$1,0 \cdot 10^{-2}$	$7,1 \cdot 10^{-5}$	$280 \cdot 10^4$
Stiffness (N/m)				
Radial	10	$3,2 \cdot 10^{-5}$	$3,16 \cdot 10^8$	
	100	$3,2 \cdot 10^{-4}$	$3,16 \cdot 10^8$	
	500	$1,6 \cdot 10^{-3}$	$3,16 \cdot 10^8$	
	1000	$3,2 \cdot 10^{-3}$	$3,16 \cdot 10^8$	
	2000	$6,3 \cdot 10^{-3}$	$3,16 \cdot 10^8$	
Axial	10	$2,6 \cdot 10^{-4}$	$3,86 \cdot 10^7$	
	100	$2,6 \cdot 10^{-3}$	$3,86 \cdot 10^7$	
	500	$1,3 \cdot 10^{-2}$	$3,86 \cdot 10^7$	
	1000	$2,6 \cdot 10^{-2}$	$3,86 \cdot 10^7$	
	2000	$5,2 \cdot 10^{-2}$	$3,86 \cdot 10^7$	